IDŐJÁRÁS

QUARTERLY JOURNAL
OF THE HUNGARIAN METEOROLOGICAL SERVICE

CONTENTS

****

http://omsz.met.hu/english/ref/jurido/jurido_en.html

VOL. 108 * NO. 3 * JULY – SEPTEMBER 2004

IDŐJÁRÁS

Quarterly Journal of the Hungarian Meteorological Service

Editor-in-Chief
LÁSZLÓ BOZÓ

Executive Editor
MARGIT ANTAL

Editorial Office: P.O. Box 39, H-1675 Budapest, Hungary or
Gilice tér 39, H-1181 Budapest, Hungary
E-mail: bozo.l@met.hu or *antal.e@met.hu*
Fax: (36-1) 346-4809

Subscription by

mail: IDŐJÁRÁS, P.O. Box 39, H-1675 Budapest, Hungary;
E-mail: bozo.l@met.hu or *antal.e@met.hu*; *Fax: (36-1) 346-4809*

IDŐJÁRÁS

Quarterly Journal of the Hungarian Meteorological Service

Editorial

I have been nominated as the Editor-in-Chief of IDŐJÁRÁS by the President of the Hungarian Meteorological Service, for the period of 2004–2008, starting with this issue of our Journal.

I graduated in meteorology from the Eötvös Loránd University in Budapest in 1986. Currently I am leading the Environmental Division of the Hungarian Meteorological Service, involved in several research issues of air pollutants' transport and dispersion modeling. I have been a member of the Editorial Board of IDŐJÁRÁS since 1997. I am taking part in the activities of international scientific communities as a member of Working Group on Environmental Pollution and Atmospheric Chemistry of WMO CAS, as a national expert of the Steering Committee of the EU Harmonization within Atmospheric Dispersion Modelling for Regulatory Purposes, and as national secretary of the International Union of Geodesy and Geophysics.

I have been principal investigator of several national, bi-lateral, and multi-lateral international scientific projects in the field of meteorology and environmental sciences for the past 15 years.

It is great honour to me to have been selected for this prestigious position at IDŐJÁRÁS, the fifth oldest meteorological journal in the world, which has now 108 years long history. It is very exciting and challenging task to follow excellent Hungarian meteorologists in this position. The scope and policy of the Journal should not be changed: to publish high quality peer reviewed papers from any parts of the world in the field of meteorology and atmosphere related scientific areas. Most of the members of the Editorial Board will continue their valuable work in realizing this goal, altogether with new experts which have recently joined the Board.

László Bozó D.Sc.

IDŐJÁRÁS

Quarterly Journal of the Hungarian Meteorological Service
Vol. 108, No. 3, July–September 2004, pp. 155–162

Estimation of the nitrogen loading from the atmospheric dry deposition of ammonium and nitrate aerosol particles to Lake Balaton

Szilvia Kugler[1]* and **László Horváth[2]**

[1]*Department of Meteorology, Eötvös Loránd University,*
P.O. Box 32, H-1518 Budapest, Hungary; E-mail: kuglersz@ludens.elte.hu

[2]*Hungarian Meteorological Service,*
P.O. Box 39, H-1675 Budapest, Hungary; E-mail: horvath.l@met.hu

(Manuscript received July 30, 2003; in final form September 17, 2003)

Abstract—The N-loading to Lake Balaton is an important cause for the observed eutrophycation. One of the most important sources of nitrogen compounds is atmospheric deposition. In this paper, the N-loading due to the dry deposition of atmospheric particles is determined. Concentrations of ammonium and nitrate ions in the particulate phase were determined on the basis of one-year bulk concentration measurements. Mean deposition velocities were estimated on the basis of *Slinn* and *Slinn* (1980) for ammonium and nitrate using the mean mass diameter of particles determined by *Mészáros et al.* (1997). From the measured concentrations and dry deposition velocities derived, a total of 11.2 ± 1.1 and 7.7 ± 0.8 mg N m^{-2} yr^{-1} N-loading were calculated for ammonium and nitrate particles, respectively. This amount is negligible in comparison with the other N-sources from the atmosphere.

Key-words: dry deposition, aerosol particles, ammonium and nitrate particles, nitrogen loading.

1. Introduction

The observed eutrophycation of Lake Balaton in the second half of the last century was the consequence of the increased nutrient (N, P) loading from various sources. Among them, the atmospheric input of the nitrogen is one of the most important factors. Since the mid-1970's numerous experiments have

*Correspondig author

been carried out to determine the rate of nutrient flux by atmospheric dry and wet deposition to the surface of Lake Balaton (e.g., *Dobolyi* and *Horváth,* 1978; *Mészáros et al.,* 1980; *Horváth et al.*, 1981; *Horváth,* 1982; *Horváth,* 1984; *Horváth,* 1990).

Investigations described in these papers have determined wet deposition based on a sampling network installed around the lake. The wet deposition rate of phosphorus and nitrogen compounds was derived from the chemical composition (concentration of N- and P-forms) and the amount of precipitation.

The estimation of the dry deposition flux is more complicated compared to the determination of the wet deposition flux. Previous studies did not take into account two important nitrogen compounds (N_2O, HNO_3). Furthermore, there are some other compounds (e.g., N_2O and NH_3) that have bi-directional flux, i.e., as a function of the physico-chemical conditions the net flux can be positive (emission) or negative (deposition). Since the rate of exchange processes controlling the nitrogen balance between the water and atmosphere strongly depends on the nitrogen loading of the water, in extreme cases the lake would be a net emitter for nitrogen compounds. In other words, a negative feed-back mechanism which results in self-cleaning of the lake can not be excluded.

In addition to the problems of gaseous N-compounds, estimation of the dry deposition of particle-phase ammonium and nitrate ions is one of the most uncertain term in the estimation of N-loading. In the earlier estimations (e.g., *Horváth et al.*, 1981) the dry deposition velocities for these particles were considered on the basis of laboratory measurements. However, there is evidence that deposition mechanism of particles onto a natural water surface with waves present is quite different (*Zufall et al.*, 1999a,b).

In summary: the nutrients carried by precipitation (wet deposition) can be easily determined. However, the prediction of the rate of dry deposition is much more difficult. According to the above mentioned reasons, even the direction of the flux of gaseous N-compounds is uncertain. On theoretical grounds, the possibility that more nitrogen compounds are released from the lake than deposited from the atmosphere cannot be excluded. Conversely, the rate of dry deposition could be higher than expected, and in extreme cases it may exceed the rate of wet deposition by orders of magnitude. The ratio of dry to wet deposition cannot be determined from the data presently available.

For the above reasons it is necessary to re-evaluate the nitrogen balance between the atmosphere and Lake Balaton on the basis of new considerations for modeling and measurement strategies. The present work aims to determine the nitrogen loading by the dry deposition of atmospheric nitrate and ammonium particles.

2. *Methods and measurements*

Dry deposition of aerosol particles is calculated with the aid of a simple model. If the flux of the particles is one-directional, i.e., the upward flux can be neglected, then the deposition model is more simple than for gases. The deposition velocity of particles strongly depends on their size distribution. The deposition rate for particles (D_d) with a diameter of d can be described by the formula: $D_d = v_d\, c_d$, where v_d is the deposition velocity, and c_d is the atmospheric concentration. In order to determine the mean deposition flux of the particles, the size distribution, the mean deposition velocity of a certain size fraction, and the concentration in the given size fraction must be known. The goal of our work is to determine these parameters. Theoretically, the integral of D_d for the whole size distribution of the aerosol particles containing nitrogen gives the total deposition. In practice, however, an average size of the particles is derived from size distribution curves. A certain dry deposition velocity value is related to a given average particle size by a function that strongly depends on the size of the particle. The product of the deposition velocity and the concentration of the particulate ammonium or nitrate in a given size range gives the rate of the dry deposition.

2.1 Measurement of nitrate and ammonium concentrations in particle phase

Ammonium and nitrate concentration in the aerosol particles was measured in samples taken at Siófok station (southern shore of Lake Balaton) at a height of 12.3 m above the water surface. Sampling period ranged from March, 2002 to February, 2003. During the sampling, total suspended aerosol particles were collected on a Teflon filter on the basis of bulk aerosol sampling in the entire size range. A NILU EK-type sequential (two-channel) sampler was used and combined with three-stage filter packs. Ammonium and nitrate particles were determined from the first (Teflon) filter. After extracting the filters, the nitrate and ammonium concentrations in the solution were analyzed by ion chromatography and spectrophotometric method. For details of sampling and analysis see: *EMEP* (1996).

Monthly averages calculated from the daily concentrations measured at the station are presented in *Table 1*. It should be mentioned here that in case of nitrate an expressed concentration minimum can be observed during summer months as a consequence of the higher volatilization rate of nitrate with the increase of temperature. It would result in parallel increase of nitric acid concentration in the atmosphere.

Table 1. The measured mean monthly ammonium and nitrate in particle phase at Lake Balaton

2002–2003	Monthly mean concentrations ($\mu g\ m^{-3}$)	
	Ammonium	**Nitrate**
March	1.97	4.11
April	1.89	2.43
May	1.00	1.16
June	0.91	0.60
July	0.80	0.54
August	1.11	0.73
September	1.34	1.58
October	1.49	2.20
November	1.55	2.18
December	2.76	2.73
January	2.68	3.02
February	4.61	6.19
Yearly mean	**1.84**	**2.29**

2.2 *Size distribution of aerosol particles*

Only a few data are available for the particle size distribution. According to observation of *Mészáros et al.* (1997), the mean mass diameter of the nitrate particles for summer and winter are 1.5 and 0.80 μm, while for ammonium these values are 0.6 and 0.8 μm, respectively. The latter experiment was carried out over a less polluted area of the town Veszprém, situated approximately 8 km north of Lake Balaton. According to the experimental results for background aerosol particles (*Horváth et al.*, 2001, 2003), the majority of the nitrate particles is in the coarse particle fraction ($d > 2.5$ μm), while the ammonium particles are in the fine particle fraction ($d < 2.5$ μm). The experimental results of different time and location are quite different, the only similarity between them is that nitrate can usually be found in the particle fraction with larger diameter. In order to calculate the dry deposition rates it is necessary to use the values resulting from the calculations of the measurements near the lake (*Mészáros et al.*, 1997). In *Table 2* the results of these measurements are compiled.

2.3 *Dry deposition velocity of particles*

There are large uncertainties in the estimation of the dry deposition velocity of aerosol particles. Most of the existing measurements, wind tunnel experiments, and theoretical calculations relate to deposition on solid surfaces. The values for deposition velocity obtained from the different methods vary with orders of

magnitude. *Ruijgork et al.* (1993); *Borrell et al.* (1997) have pointed out that the deposition velocity determined theoretically or on the basis of laboratory measurements are much lower than those obtained from field measurements. It is evident that deposition velocities determined for the areas covered with vegetation are different from those over water surfaces. The deposition rates are different due to differences in the roughness parameter and the relative humidity above the water surfaces. The paper of *Slinn* and *Slinn* (1980) demonstrates that the deposition velocity above water surfaces depends mainly on the characteristics of the particle especially their hygroscopic or non-hygroscopic nature. In our calculations the values given by the above authors for hygroscopic particles were used at 5 m s^{-1} wind speed and 99% relative humidity above the water surface. The deposition velocities used for Lake Balaton are presented in *Table 2*, indicating the strong dependence on average particle diameter.

Table 2. Mean concentration, particle diameter, dry deposition velocity, and dry deposition of ammonium and nitrate particles (summer half year: April–September; winter half year: October–March)

Ammonium				
Period	**Concentration** ($\mu g\ m^{-3}$)	**Mean particle diameter** (μm)	**Deposition velocity** ($cm\ s^{-1}$)	**Dry deposition** ($mg\ N\ m^{-2}$)
Summer half	1.18	0.6	0.016	2.3
Winter half	2.51	0.8	0.029	8.9
Year	**1.84**	–	–	**11.2**

Nitrate				
Period	**Concentration** ($\mu g\ m^{-3}$)	**Mean particle diameter** (μm)	**Deposition velocity** ($cm\ s^{-1}$)	**Dry deposition** ($mg\ N\ m^{-2}$)
Summer half	1.17	1.5	0.1	4.2
Winter half	3.41	0.8	0.029	3.5
Year	**2.29**	–	–	**7.7**

3. Results: estimation of the dry deposition rate for nitrate and ammonium particles

The most important data concerning the deposition rate of the ammonium and nitrate particles are presented in *Table 2*. The second column gives the mean concentrations that were determined as described in paragraph 2.1. The third column shows the average particle diameters determined as described in

paragraph 2.2, while the fourth column gives the values determined from *Slinn* and *Slinn* (1980). From these data, dry deposition values were calculated as given in the last column. The uncertainty of these figures can be estimated as the bulk error of sampling and analysis of nitrate and ammonium concentrations. The estimated bulk relative error for filter pack sampling and analysis is between 5–10% (*Horváth et al.*, 2003).

Taking into account these uncertainties, the ammonium and nitrate particle deposition onto Lake Balaton are 11.2 ± 1.1 and 7.7 ± 0.8 mg N m^{-2} yr^{-1}. The total N-deposition from atmospheric particles is 18.9 ± 1.9 mg N m^{-2} yr^{-1}. The ammonium and nitrate loading for the whole surface of the lake is 11.2 ± 1.1 t N yr^{-1} assuming a surface area of 595 km^2. This rate is likely negligible in comparison with the total nitrogen loading determined on the basis of previous measurements (*Horváth et al.*, 1981). In that paper a total of 590 t N yr^{-1} for the nitrogen loading to Lake Balaton was reported, that is higher by two orders of magnitude than the dry deposition of ammonium and nitrate particles estimated here. The difference is obviously due to wet deposition of nitrate and ammonium ions. It is difficult to give an estimation for the total N-budget between the lake and the atmosphere in the lack of knowledge of ammonia, nitrous oxide, and nitric acid dry fluxes. Investigation of these processes will be a task for the future, but dry flux of nitrogen compounds in particle phase probably does not play an important role in nitrogen loading.

The probability of a long-term variation in N-loading by aerosol particles can be estimated from the long-term variation of concentrations. Long term concentration data from the nearest background air pollution monitoring station (K-puszta, 150 km east of Siófok) shows the large variation between the years (*Fig. 1*). During the last 15–20 years, changes in ammonium and nitrate concentration have been within a factor of about two. It is difficult to predict future variability, but it is likely that considerable changes can not be expected in concentrations and, therefore, in the deposition of N-containing particles.

3. Conclusion

According to the experiments, theoretical considerations, and literature data, we can conclude that the dry flux of ammonium and nitrate aerosol particles to the lake surface are 11.2 ± 1.1 and 7.7 ± 0.8 mg N m^{-2} yr^{-1}. According to the long term changes of concentrations, these rates are not expected to change considerably in the near future. The ammonium and nitrate load for the whole lake is 11.2±1.1 t N yr^{-1}. This amount of load is likely negligible in comparison to the total nitrogen flux determined on the basis of previous

measurements (*Horváth et al.*, 1981). In the future, when the balance of gases (ammonia, nitrous oxide, nitric acid) will be better known, the yearly loading of N-compounds is subject to changes, but it is probable that deposition of aerosol particles does not carry nitrogen to the lake in substantial quantity.

Acknowledgements—Investigations has been sponsored by the Ministry of the Environment, Hungary. We wish to thank the personnel of Siófok observatory for their help in sampling.

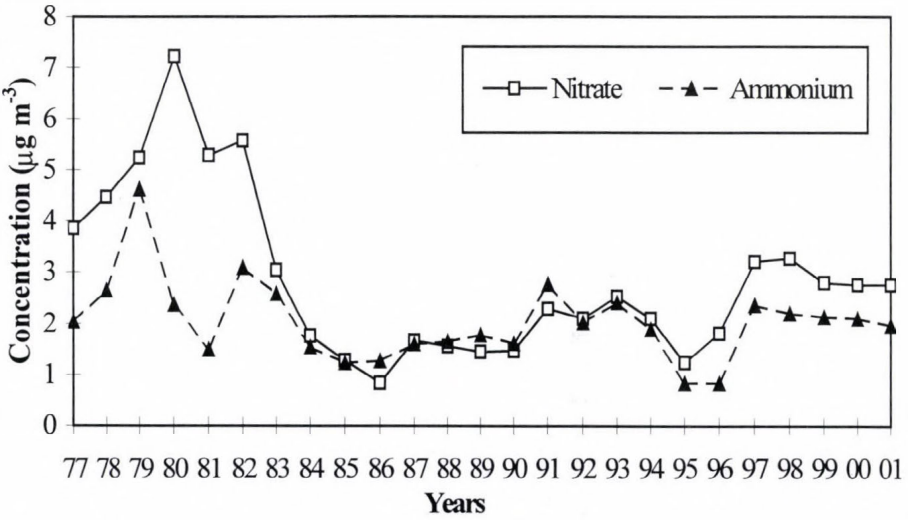

Fig. 1. Long term variation of nitrate and ammonium concentration in particles, K-puszta station.

References

Borrell, P., Builtjes, J.H., Grennfelt, P., and *Hov, O.* (eds.), 1997: *Transport and Chemical Transformation of Pollutants in the Troposphere, 10. Photo-Oxidants, Acidification and Tools: Policy Applications of EUROTRAC Results*. Springer-Verlag, Berlin, Heidelberg, 116 pp.

Dobolyi, E. and *Horváth, L.*, 1978: Investigation of the amount of direct nutrient (P, N) loading from the atmosphere to Lake Balaton (in Hungarian). *Hidrológiai Közlöny 12*, 547-552.

EMEP, 1996: EMEP co-operative program for monitoring and evaluation of the long-range transmission of air pollutants in Europe. EMEP Manual for sampling and chemical analysis. *EMEP/CCC-Report 1/95*, NILU, Kjeller, Norway.

Horváth, L., 1982: On the vertical flux of gaseous ammonia above water and soil surfaces. In *Deposition of Atmospheric Pollutants*. D. Reidel Publishing Company, Dodrecht, pp. 17-22.

Horváth L., 1984: Effect of the air pollution on the water quality of Lake Balaton (in Hungarian). OKKFT A/12 "Regional environmental protection research of Lake Balaton". *OKTH Környezet- és természetvédelmi kutatások* 3, 161-162.

Horváth L., 1990: Concentration and deposition of airborne pollutants in the catchment of Lake Balaton (in Hungarian). *Vízügyi Közlemények 77*, 204-208.

Horváth, L., Mészáros, Á., Mészáros, E., and *Várhelyi, G.*, 1981: On the atmospheric deposition of nitrogen and phosphorus into Lake Balaton. *Időjárás 85*, 194-200.

Horváth, L., Mészáros, R., Pinto, J.P., and *Weidinger, T.*, 2001: Estimate of the dry deposition of atmospheric nitrogen and sulfur species to Spruce forest. In *Proc. of EUROTRAC Symposium 2000* (eds.: *P.M. Midgley, M. Reuther*, and *M. Williams*). *Garmish-Partenkirchen, Germany*, 27-31 March 2000. Springer-Verlag, Berlin, Heidelberg.

Horváth, L., Pinto, J., and *Weidinger, T.*, 2003: Estimate of the dry deposition of atmospheric nitrogen and sulfur species to spruce forest. *Időjárás 105*, 249-255.

Mészáros, E., Horváth, L., Mészáros, Á., and *Várhelyi, G.*, 1980: Effect of the air pollution on the water quality of Lake Balaton (in Hungarian). *MTA/VEAB Monográfiái 6*, 87-101.

Mészáros, E., Barcza, T., Gelencsér, A., Hlavay, J., Kiss, Gy., Krivácsi, Z., Molnár, Á. and *Polyák, K.*, 1997: Size distributions of inorganic and organic species in the atmospheric aerosol in Hungary. *J. Aerosol Sci. 28*, 1163-1175.

Ruijgork, W., Nicholson, K.W., and *Davidson, C.I.*, 1993: Dry deposition of particles. In *Models and Methods for the Quantification of Atmospheric Input to Ecosystems*. Nordiske Seminar og Arbejdsrapporter 1993: 573. Nordic Council of Ministers, Copenhagen, 145-161.

Slinn, S.A. and *Slinn, W.G.N.*, 1980: Prediction for particle deposition on natural waters. *Atmos. Environ. 14*, 1013-1016.

Zufall, M.J., Dai, W., Davidson, C.I. and *Etyemezian, V.*, 1999a: Dry deposition of particles to wave surfaces: I. Mathematical modeling. *Atmos. Environ. 33*, 4273-4281.

Zufall, M.J., Dai, W., and *Davidson, C.I.*, 1999b: Dry deposition of particles to wave surfaces: II. Wind tunnel experiments. *Atmos. Environ. 33*, 4283-4290.

IDŐJÁRÁS

Quarterly Journal of the Hungarian Meteorological Service
Vol. 108, No. 3, July–September 2004, pp. 163–171

Analysis of the extremity of precipitation intensity using the POT method

Mónika Lakatos[1]* and **István Matyasovszky**[2]

[1]*Hungarian Meteorological Service,*
P.O. Box, 38, H-1525 Budapest, Hungary; E-mail: lakatos.m@met.hu

[2]*Department of Meteorology, Eötvös Loránd University,*
P.O. Box 32, H-1518 Budapest, Hungary; E-mail: matya@ludens.elte.hu

(Manuscript received March 16, 2004; in final form July 16, 2004)

Abstract—The paper presents a procedure going beyond the classical extreme value analysis of data sets considering only one extreme value per year. The main advantage of the Peaks Over Threshold (POT) method is to use every data exceeding a specified high, or staying under a specified low threshold. The methodology is used to estimate return levels. A return level is defined as a level, which is exceeded in average one time during a specified period. The procedure is applied to a data set consisting of 10-minute precipitation amounts at Baja-Csávoly, Hungary, for the period from 1997 to 2003.

Key-words: short-term precipitation, extremes, POT method, generalized Pareto distribution, return levels.

1. Introduction

The measuring practice of short-term precipitation has completely changed with installing automatic climate stations. In the period preceding the automatization, ombrographs registered the quantity of precipitation. Evaluation of the rain register paper was carried out by selecting the largest precipitation amounts during 5, 10, 20, 30, 60, 180 min periods within a wet event, considering the slope of the curve of accumulated precipitation and registering these partial amounts. In the national observing network *Váradi* and *Nemes* (1992) performed a statistical analysis of data registered by

* Corresponding author

ombrographs for 26 stations in Hungary for the period from 1967 to 1991. Besides frequency histograms, extreme value analysis was also made for the maxima of different time intervals using a procedure developed by *Faragó* (1990). This program fits the GEV distribution to maxima and results in the return levels for different return periods.

Automatic stations replaced the ombrographs in many places in Hungary making the short term sampling possible. At the Hungarian Meteorological Service the amount of precipitation is registered every ten minutes forming a data set for further analysis. This paper reports an examination of extreme large ten minutes precipitation amounts. Section 2 presents the methodology based on the so-called POT technique. Section 3 summarizes the main results. Finally, a section is provided for conclusions.

2. POT method

Extreme value analysis is generally based on asymptotic formulae. Under general conditions, the maximum of a sample is described by the Jenkinson distribution, which includes the three possible types of the probability distribution of maxima, namely the Gumbel, Fréchet and Weibull distributions. This is a successful way, when a quite large sample is available for the maximum. However, the method cannot be applied when the maximum of an N length period is in question, and observations cover an n length period, where n is not much larger than N. Also, even an appropriate sample size is available there is a chance that the largest value from an n length period is smaller than the second largest value from an other period.

Therefore, it looks promising to use every observation representing large values. The concept includes a specification of a high threshold and peaks over threshold (POT), i.e., threshold excesses are used in the analysis. Modeling of threshold excesses has been first applied to hydrological problems. Statistical properties of this approach are detailed in *Davison* and *Smith* (1990). Description of the POT method and other techniques to analyze extreme values is summarized in *Coles* (2001). Results obtained with the POT method and GEV model are compared for Palmer Drought Severity Index for several Hungarian meteorological stations (*Zempléni et al.*, 1999).

2.1 Generalized Pareto distribution

Let X be a random variable with probability distribution function F. Taking a threshold w, the conditional probability

$$P(X > w + y \mid X > w) = \frac{1 - F(w+y)}{1 - F(w)}, \qquad y > 0, \tag{1}$$

could be easily calculated if F were known. Because the distribution function is not known as accurately as required for using Eq. (1), an asymptotic approximation is used in practice. Under general conditions (*Leadbetter et al.*, 1983), the Eq. (2) approximates Eq. (1) for high thresholds:

$$P(X > w + y \mid X > w) = \frac{1 - F(w+y)}{1 - F(w)} = \left[1 + \frac{\xi y}{\sigma}\right]^{-1/\xi} = 1 - H(y), \tag{2}$$

where $H(y)$ is the generalized Pareto distribution function

$$H(y) = 1 - (1 + \frac{\xi y}{\sigma})^{-1/\xi}, \qquad y > 0, \qquad (1 + \xi y/\sigma) > 0. \tag{3}$$

When the shape parameter ξ is zero, the Pareto distribution becomes exponential distribution with parameter $1/\sigma$:

$$H(y) = 1 - \exp(-\frac{y}{\sigma}), \qquad y > 0. \tag{4}$$

Note that ξ does not depend on w but the scale parameter σ does.

Choice of the threshold has a crucial role in application. When taking a too low threshold, the Pareto distribution is a poor approximation to Eq. (1), and thus the model is biased. Also, even observations X_i, $i = 1,...n$, are not independent, the excesses $X_i - w > 0$ tend to be independent as w tends to infinity. However, a too high threshold delivers a small number of observations exceeding this threshold and results in a large variance of the estimated parameters. Therefore, the threshold must not be too high.

There are two ways of the threshold selection. The first is to estimate the threshold too, while the second way is to fit Pareto distributions with different thresholds and analyze the stability of estimated parameters. In the first case, it is utilized that $\mathrm{E}[X - w \mid X > w]$ is a linear function of w. Thus, substituting the conditional expected values by corresponding means, the threshold is chosen as the minimum of candidate values of w, which satisfies the linear dependence of means on w. In the second case, the threshold is chosen such that estimates of ξ under different values of w fluctuate around a constant.

2.2 *Parameter estimation*

With $y_i = X_i - w$, $X_i > w$, $i = 1,...,k$ the log-likelihood function

$$l(\sigma,\xi) = -k\log\sigma - (1+1/\xi)\sum_{i=1}^{k}\log(1+\xi_i/\sigma), \quad 1+\xi_i y_i/\sigma > 0, \tag{5}$$

has to be maximized with respect to σ and ξ. Numerical techniques are required for the purpose taking care to avoid numerical instabilities when $\xi \approx 0$. In the case of $\xi = 0$, the log-likelihood is

$$l(\sigma) = -k\log\sigma - \sigma^{-1}\sum_{i=1}^{k} y_i .$$

2.3 *Return levels*

The degree of extremity can be characterized by return levels. A return level x_m is defined as a level, which is exceeded in average one time during an m length period. Due to this definition and considering Eq. (3),

$$P(X > x_m) = p_w\left(1+\xi\left(\frac{x_m - w}{\sigma}\right)\right)^{-1/\xi} = 1/m \tag{6}$$

is solved for x_m, where $p_w = P(X > w)$. In the solution:

$$x_m = w + \frac{\sigma}{\xi}\left[(mp_w)^{\xi} - 1\right], \tag{7}$$

the parameters are substituted by their maximum likelihood estimates, $\tilde{\xi},\tilde{\sigma}$, and $\tilde{p}_w = k/n$.

In the case of $\xi \approx 0$, Eq. (4) leads to $x_m = w + \sigma\log(mp_w)$.

2.4 *Model verification*

Graphical methods are generally used to check suitability of the fitted Pareto distributions. Having an ordered sample $y_{(1)} \le ..... \le y_{(k)}$ used to fit a Pareto model, the relative frequencies $\{i/(k+1); i = 1,\ldots,k\}$ and model-generated $\{\tilde{H}(y_{(i)}); i = 1,\ldots,k\}$ estimates of probabilities $\{P(X - w \mid X > w) < y_i; i = 1,\ldots,k\}$

should be close to each other. Therefore, the points $\{(i/(k+1), \widetilde{H}(y_{(i)})); i = 1,\ldots,k\}$ will fluctuate around a line when the model is appropriate (probability plot).

Another approach, the quantile plot, considers the points $\{(\widetilde{H}^{-1}(i/(k+1)), y_{(i)}); i = 1,\ldots,k\}$, because they will scatter around a line when the model is appropriate.

3. Example

The data set consists of 10-minute precipitation amounts for Baja-Csávoly (φ=46°11', λ=19°01'), for the period from 1997 to 2003. The automatic rain gauge was installed earlier, but reliable and continuous data are available since 1997. Months of the year were analyzed separately due to the strong annual cycle. Thus, Pareto distributions were fit for each month using an Splus program of *Coles* (2001).

The first and very important step of the model building is the selection of suitable thresholds as it was mentioned in Section 2. A properly selected threshold considers two requirements. Namely, the threshold w is enough high to satisfy the statistical independence of threshold excesses, but enough low to have a satisfactory amount of threshold excesses to estimate model parameters with moderate variances. This procedure is demonstrated with July, because this is a typical period of short and intensive rainfall events in Hungary.

A diagnostic procedure using the modified scale parameter, $\sigma^* = \sigma_w - \xi w$, and shape parameter ξ can help in the threshold selection. *Fig. 1* shows these parameters with their confidence intervals of 95% against the threshold. The lowest threshold w has to be chosen, which satisfies that the above-mentioned parameters may be considered constants for higher values of w. Note that both σ^* and ξ show an apparent change around w = 1 mm, but stabilize over 1.2 mm. As it is crucial that enough number of threshold excesses are available for the estimation procedure, a threshold larger than 1 mm does not seem a good choice. Because at w = 1 mm the number of excesses is 97, and a considerably higher threshold delivers drastically smaller number of such cases (see *Fig. 2*), our final choice is 1 mm in July. Excesses corresponding to this choice have been tested for statistical independence using a test based on the sign of neighboring sample elements (*Kendall* and *Stuart,* 1966). The independence is acceptable at least at 0.01 significance level. This procedure was applied for each month, and the selected thresholds are shown in *Table 1*. These values are obviously larger for summer than winter, due to the more intensive precipitation in the warm season. However, the low thresholds in winter appear quite, high because considerably fewer excesses are available than in

summer. This is because relatively high thresholds had to be chosen to satisfy the statistical independence of excesses.

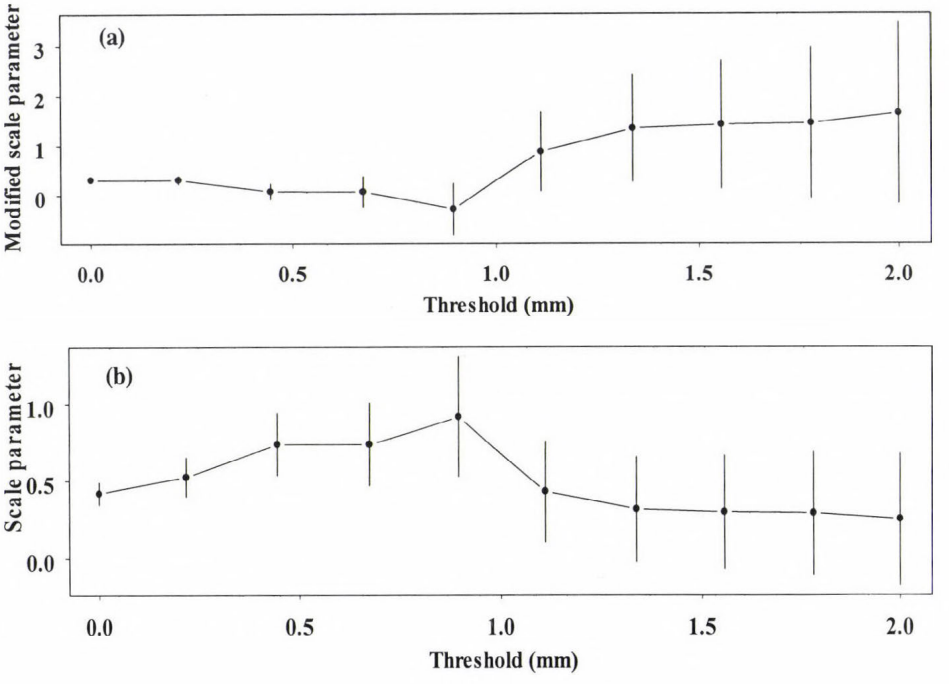

Fig. 1. Modified scale ($\sigma^* = \sigma_u - \xi$) (*a*) and scale parameter ξ (*b*) against w of the Pareto distribution fitted to July data.

Having the thresholds, the scale and shape parameters are estimated by maximizing Eq. (5). In the case of July, the estimated parameters of the Pareto fitting are $\sigma = 1.405$ and $\xi = 0.383$. Return levels obtained from Eq. (7) are also shown in *Table 1*, for 2, 5, 10, 50, and 100 years return periods. As it is expected, the highest values are in summer and lowest ones are in winter. Comparing the 5 and 10 years return levels with the observed 7-year maximum, the values estimated by Eq. (7) look underestimated. For instance, the observed 7-year maximum in January is 1.9 mm corresponding to the 50-year return level. Such underestimation does not appear in summer suggesting the effect of few threshold excesses in winter. For December the Pareto fitting leads to $\xi = 0.01$, so the exponential distribution seemed to be a good approximation of Eq. (4).

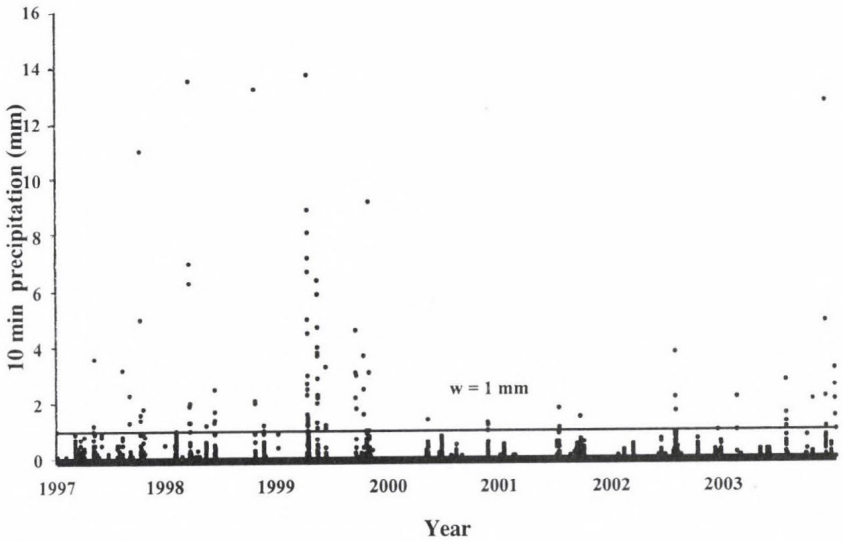

Fig. 2. 10 min precipitation sums and the selected $w = 1$ mm threshold for July, in the period 1997–2003.

Table 1. Selected thresholds and return levels for each month

Month	Threshold w (mm)	Return period (year)					
		2	5	10	50	100	
January	0.5	1.2	1.4	1.6	1.9	2.0	
February	0.5	1.5	1.9	2.4	3.5	4.1	
March	0.6	1.4	1.6	1.7	1.8	1.8	
April	0.7	1.8	2.0	2.2	2.5	2.6	
May	0.7	3.3	4.5	5.7	9.1	11.0	
June	0.9	6.5	9.4	12.3	22.0	28.0	
July	1.0	10.6	16.2	22.0	43.5	57.7	
August	0.6	6.7	11.0	15.7	35.1	49.5	
September	0.7	4.0	5.7	7.3	12.7	16.0	
October	0.6	3.5	5.1	6.8	13.0	17.2	
November	0.7	1.8	2.3	2.8	4.1	4.8	
December	0.6	1.1	1.3	1.5	1.9	2.0	

Return level (mm)

Return levels with confidence intervals of 95% are presented on a logarithmic scale for July in *Fig. 3.* Empirical estimates of the sample elements are also shown in the return level plots. Evidently, the confidence interval

becomes wider as return period increases. Because the observed 7-year maximum in July is 13.7 mm, the values shown in *Table 1* probably overestimate the return levels in this month.

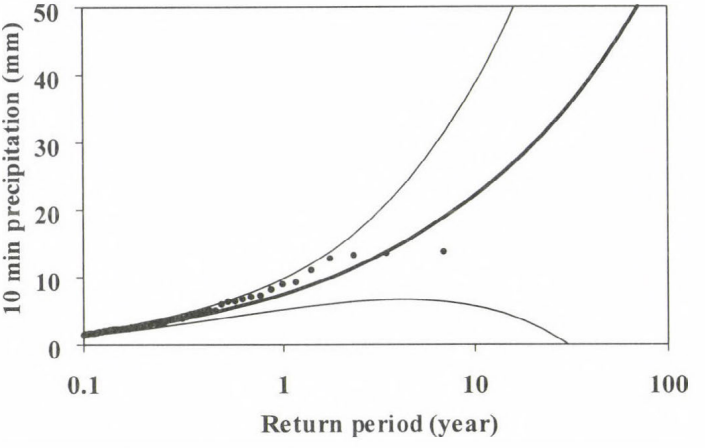

Fig. 3. Return levels and 95% confidence intervals to the different return period for July.

Diagnostic plots for the fitted generalized Pareto distribution are shown in *Fig. 4a* and *b*. The probability plot (*Fig. 4a*) for July data is approximately linear, while the goodness-of-fit considering the quantile plot (*Fig. 4b*) seems less convincing, because there are very large uncertainties at high levels.

4. Conclusions

The purpose of this paper was to present a procedure going beyond the classical extreme value analysis of data sets, taking into account only one extreme value per year. The main advantage of POT method is to use every data exceeding a specified threshold. This threshold, however, has a crucial role, and its choice is a trade-off between the bias and variance of the model. Also, statistical independence of threshold excesses should be satisfied by the choice. This problem is reflected by underestimated return levels in winter.

It may be useful to analyze short-term precipitation extremes for further intervals, e.g., for 20 min and 30 min. Also, there is a need to develop a procedure establishing a relationship between data registered with the former practice and data measured with automatic instruments.

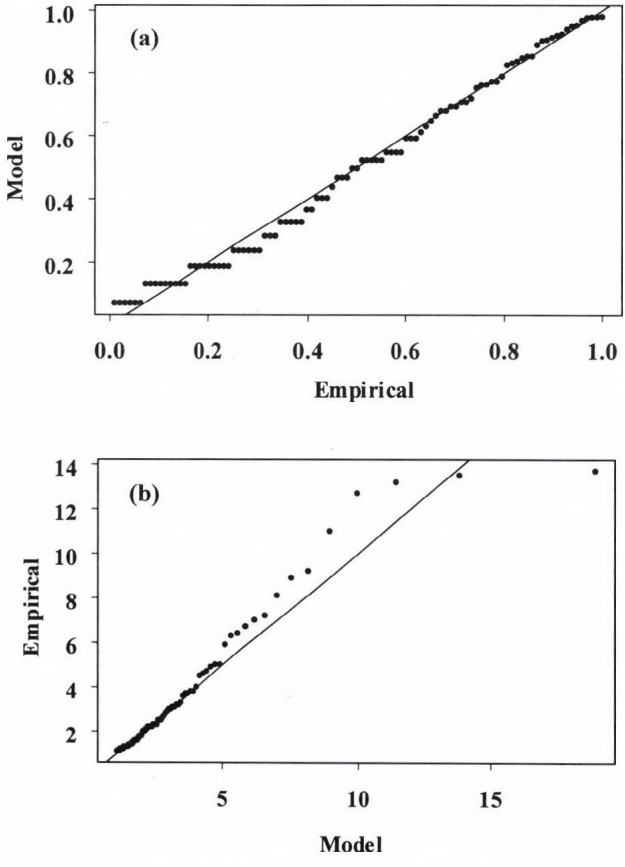

Fig. 4. Probability plot (*a*) and quantile plot (*b*) of July data.

References

Coles, S.G., 2001: *An Introduction to Statistical Modeling of Extreme Value*. Springer-Verlag, New York .

Davison, A.C. and *Smith, R.L.*, 1990: Models for exceedances over high thresholds. *J. Roy. Stat. Soc. B 52*, 393-442

Faragó, T. and *Katz, R.W.*, 1990: Extremes and design values in climatology. *WMO, TD-No. 386*, Geneva.

Leadbetter, M.R., Lindgren, G., and *Rootzen, H.*, 1983: *Extremes and Related Properties of Random Sequences and Processes*. Springer-Verlag, New York.

Váradi, F. and *Nemes, Cs.*, 1992: Frequencies of short-term precipitation in Hugary (in Hungarian). *Légkör XXXVII* (3), 8-13.

Zempléni, A.Z., Bermundez, P., and *Csiszár, V.*, 1999: Applying extreme value models for PDSI drought severity index series in Hungary (in Hungarian). *Meteorológiai Tudományos Napok*. Országos Meteorológiai Szolgálat, Budapest, 57-69.

IDŐJÁRÁS

Quarterly Journal of the Hungarian Meteorological Service
Vol. 108, No. 3, July–September 2004, pp. 173–194

Connections between urban heat island and surface parameters: measurements and modeling

János Unger[1], Zsolt Bottyán[2], Zoltán Sümeghy[1] and Ágnes Gulyás[1]

[1]*Department of Climatology and Landscape Ecology, University of Szeged, P.O. Box 653, H-6701 Szeged, Hungary*

E-mail: unger@geo.u-szeged.hu; sumeghy@geo.u-szeged.hu; agulyas@geo.u-szeged.hu

[2]*Department of Resource Economy, University of Debrecen, P.O. Box 10, H-4015 Debrecen, Hungary, E-mail: zbottyan@helios.date.hu*

(Manuscript received May 5, 2003; in final form September 26, 2003)

Abstract—This study deals with the influence of urban surface factors on the air temperature patterns, using mobile measurements under different weather conditions in the periods of March 1999 – February 2000 and April – October 2002. The studied city (Szeged, Hungary) is located on a plain with a population of 160,000. Investigations concentrated on the urban heat island (UHI) at its strongest development during the diurnal cycle. Tasks included: (1) Determination of spatial distribution of UHI intensity and some urban surface parameters (built-up and water surface ratios, sky view factor, building height). (2) Development of statistical models in the heating and non-heating seasons using the above mentioned parameters and their areal extensions. (3) Identification of similarities or differences in the seasonal spatial patterns of UHI along an urban cross-section and explanation these features using land-use and climatological parameters.

In both seasons the spatial distribution of UHI intensity fields has a concentric shape with some local irregularities. The intensity reaches more than 2°C (heating season) and 3°C (non-heating season) in the centre. According to the model equations determined by stepwise multiple linear regression analysis, there are clear connections between the spatial distribution of the urban excess temperature and the examined land-use parameters. Among these parameters sky view factor and building height are the most determining factors, which are in line with the urban surface energy balance. Along the cross-section the UHI intensity has a seasonal change, as a consequence of the prevailing weather conditions. The role of cloudiness and wind speed is clearly recognized during most of the time in the studied period. Utilization of normalized values shows that the form of the seasonal UHI profile is independent of the seasonal climatological conditions, and is determined by urban surface factors to a high degree.

Key-words: urban heat island, spatial and seasonal patterns, statistical model equations, urban cross-section, seasonal profiles.

1. Introduction

Urbanization modify materials, structure, and energy balance of the surface and air composition compared to the natural surroundings. As a consequence of the effects of these artificial factors, a distinguished local climate (urban climate) develops in the cities, which manifests itself by the excess temperature (urban heat island – UHI) most obviously. The magnitude of this excess is the UHI intensity (namely ΔT, the temperature difference between urban and rural areas). Generally, in its diurnal cycle the strongest development occurs 3–5 hours after sunset.

Simulation of real factors and physical processes generating the urban climate is difficult because of the complicated urban terrain with regard to surface geometry and materials, as well as artificial production of heat and air pollution. The detection of these factors and processes demands complex and expensive instruments, and sophisticated numerical and physical models. Despite these difficulties, several models have been developed for small-scale climate variations within the city. Some of these models are based on advective (*Oke*, 1976), energy balance (*Tapper et al.*, 1981; *Johnson et al.*, 1991; *Myrup et al.*, 1993; *Ruffieux*, 1995), radiation (*Voogt* and *Oke*, 1991), heat storage (*Grimmond et al.*, 1991), water balance (*Grimmond* and *Oke*, 1991), and surface sensible heat flux (*Voogt* and *Grimmond*, 2000) approaches. In order to study microclimate alterations within the city, utilization of statistical modeling may provide useful quantitative information about the urban temperature excess by employing different surface parameters (e.g. *Outcalt,* 1972; *Oke*, 1981, 1988; *Park*, 1986, 1987; *Kuttler et al.*, 1996; *Matzarakis et al.*, 1998).

Our objective is to investigate the seasonal effects and interactions inside the city on the air temperature, a few hours after sunset, when the UHI effect is generally most pronounced. To achieve this aim, we construct horizontal isotherm maps to show the average spatial distribution of the UHI intensity in the investigated periods and present some obvious relationships between temperature patterns and urban factors. Then we examine the quantitative effects of the relevant surface factors and their combinations on the patterns of the urban-rural temperature differences. The selection of these parameters, namely built-up ratio, water surface ratio, sky view factor, and building height, is based on their role in small-scale climate variations (*Oke*, 1987; *Golany*, 1996). Finally, we identify similarities or differences in the spatial distributions of ΔT by seasons along an urban cross-section and explain these features using land-use and climatological parameters.

2. Environmental conditions

The studied city, Szeged, is located in the south-eastern part of Hungary (46°N, 20°E) at 79 m above sea level on a flat flood plain. River Tisza passes through the city, otherwise, there are no large water bodies nearby. The river is relatively narrow and, according to our earlier investigation, its influence is negligible (*Unger et al.* 2000, 2001). These environmental conditions make Szeged a suitable place for studying an almost undisturbed urban climate.

Most of Hungary belongs to Köppen's climatic region Cf (temperate warm climate with a fairly uniform annual distribution of precipitation). Climatic subregions are distinguished using the mean temperature of vegetative season (t_{VS} in °C) and the aridity index ($H = Q^*/L_V P$ where Q^* is the annual mean net radiation in MJ m^{-2}, L_V is the latent heat of evaporation in MJ kg^{-1} and P is the annual mean precipitation in kg m^{-2}). The climate is arid or humid, according to whether the dimensionless H is bigger or less than 1, respectively. Szeged is in the *warm-dry* subregion by this classification, which is characterized by $t_{VS} > 17.5$°C and $H > 1.15$ (*Unger*, 1999). Two half years can be distinguished from the point of view of city dwellers: the heating (from October until April) and the non-heating (from April until October) seasons.

Szeged has an administration district of 281 km^2 with a population of 160,000. The base of the street network is a circuit-avenue system. Different land-use types are present including a densely-built centre with medium-wide streets and large housing estates of high concrete buildings set in wide green spaces. There are zones used for industry and warehousing, areas occupied by detached houses, considerable open spaces along the riverbanks, in parks, and around the city's outskirts (*Unger et al.*, 2000).

3. Parameters and methods

3.1 Grid network

Our efforts were focused on the urbanized part of the administration district. The area of investigation was divided into two sectors and subdivided further into 0.5 km × 0.5 km square cells (*Fig. 1*). The same grid size was employed, for example, in an investigation of UHI in Seoul, Korea (*Park*, 1986). The original study area consists of 107 cells covering the urban and suburban parts of Szeged, mainly inside of the circle dike that protects the city from river floods. The outlying parts, characterized by mostly rural features, are not included in the network except for four cells on the western side of the area, which are necessary to determine the temperature contrast between urban and

rural areas. The grid was established by quartering the 1 km × 1 km square network of 1:10,000 scale maps of the Unified National Mapping System developed for the topographical maps of Hungary (*Unger et al.*, 2000, 2001).

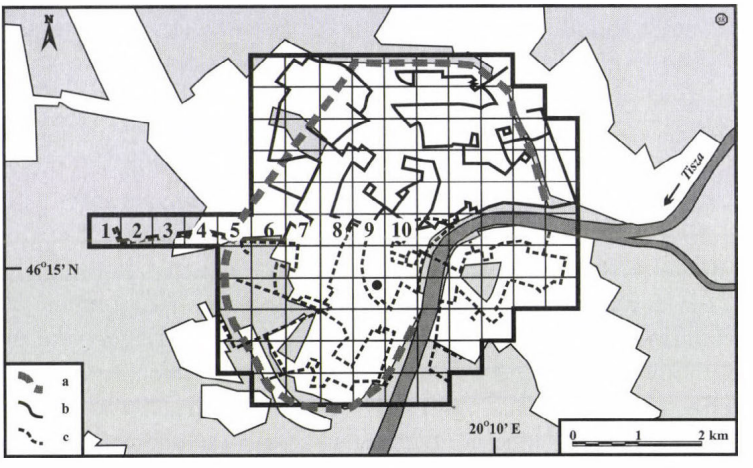

Fig. 1. Division of the area of study into 0.5 km × 0.5 km grid cells. The dashed line (*a*) denotes the circle dike, (*b*) and (*c*) are the measurement routes in the northern and southern sectors, respectively. The permanent measurement site of the University of Szeged is indicated as •, and the cells of cross-section are numbered from 1 to 10.

In the present research, six southern and four western cells of the original study area are omitted because of the lack of one parameter in the data set (building height, see Section 3.5). Therefore, we employ altogether 97 cells covering an area of 24.25 km^2.

3.2 Temperature (maximum UHI intensity)

In order to collect data on ΔT for every cell, mobile measurements were performed on fixed return routes once a week during the period of March 1999–February 2000 (*Fig. 1*). In case of surface and near-surface air UHI measurements, vehicle-based observation (car, tram, helicopter, airplane, satellite) is a common process (e.g., *Conrads* and *van der Hage*, 1971; *Oke* and *Fuggle*, 1972; *Johnson*, 1985; *Moreno-Garcia*, 1994; *Yamashita*, 1996; *Voogt* and *Oke*, 1997; *Klysik* and *Fortuniak*, 1999). Altogether 48 car traverses were taken, 24 in the northern, and another 24 in the southern sector. The frequency of traverses provided sufficient information under different weather conditions, except for rain.

Division of the area of the study into two sectors was necessary because of the large number of cells. The 75 km and 68 km long return routes in the northern and southern sectors, respectively, were needed to make time-based corrections, since measurements took about 3 hours. Temperature readings were obtained using a radiation-shielded resistance sensor connected to a data logger for digital sampling. Data were collected every 16 sec, so at an average car speed of 20–30 km h^{-1}, the average distance between measuring points was 89–133 m. In order to avoid the influence of engine and exhaust heat, the sensor was mounted 0.60 m in front of the car at 1.45 m above the ground. The speed was sufficient to provide adequate ventilation for the sensor to measure the ambient air temperature. The traffic density in the late hours of measurements was rather low. The logged values at forced stops (e.g., at traffic lamps) were rejected from the data set.

Having averaged the measurement values by cells, time adjustments to a reference time were applied assuming linear air temperature change with time. This change was monitored by the continuous records of the automatic weather station of the University of Szeged (*Fig. 1*). The linear adjustment appears to be correct for data collected a few hours after sunset in urban areas. However, because of the different time variations of cooling rates, it is only approximately correct for suburban and rural areas (*Oke* and *Maxwell*, 1975). The reference time, namely the likely time of the occurrence of the strongest UHI in the diurnal course, was 4 hours after sunset, a value based on earlier measurements. Consequently, we can assign one temperature value to every cell in the northern sector or in the southern sector at a given measuring night. These values refer to the centre of each cell.

UHI intensities were determined by cells referring to the temperature of the westernmost cell (1) of the original area of the study ($T_{cell} - T_{(1)}$), which was regarded as a rural cell because of its location outside of the city (*Fig. 1*). Moreover, the weather station of the Hungarian Meteorological Service is located there, and its records were used as rural (reference) data in the earlier studies on the urban climate of Szeged (e.g., *Unger*, 1996, 1999).

The 97 points (the above mentioned cell centerpoints) covering the urban parts of Szeged provide an appropriate basis to interpolate isolines (temperature and other parameters) using a geostatistical gridding method, the standard Kriging procedure.

3.3 Built-up and water surface ratio

Ratios of the built-up (covered surface – building, street, pavement, parking lot, etc.) (*B*) and water surface (*W*) by cells were determined by a vector and raster-based GIS database combined with remote sensing analysis of SPOT XS

images. The digital satellite image was rectified to the Unified National Mapping System using 1:10,000 scale maps. The nearest-neighbour method of resampling was employed, resulting in a root mean square value of less than 1 pixel. The geometric resolution of the image was 20 m × 20 m.

Normalized Difference Vegetation Index was calculated from the pixel values, using visible (0.58–0.68 μm) and near infrared (0.72–1.1 μm) bands (*Gallo* and *Owen*, 1999). They are between −1 to +1 indicating the effect of green space in the given spatial unit. Using these values, built-up, water, and vegetated surfaces were distinguished and their ratios (to total cell area) for each grid square were determined using cross-tabulation (*Unger et al.*, 2000). In the Szeged region the occurrence of non-vegetated (bare) areas is negligible, namely, each non-built-up place is covered by some vegetation (e.g., garden and cultivated plants, trees, grass, bushes, weeds).

3.4 Sky view factor

The built-up ratio does not describe completely the characteristics of an artificial urban surface. Streets and buildings create canyons, and this 3D geometry plays an important role in the development of UHI. Namely, heat transport and outgoing long wave radiation decrease because of the moderated turbulence and increased obstruction of the sky.

To estimate the openness of the cell surfaces quantitatively, we applied the sky view factor (*SVF*, now marked shortly by *S*). It is a dimensionless measure (between 0 and 1) of the degree to which sky is obscured by the surroundings for a given point (*Oke*, 1981, 1988). Commonly, *S* is determined using either analytical or photographic methods, employing theodolite, fish-eye lens (digital) camera, or automatic canopy analyzer (*Oke*, 1981; *Bärring et al.*, 1985; *Park*, 1987; *Grimmond et al.*, 2001).

In our analytical method we have measured two elevation angles to the top of the buildings (α_1 and α_2) perpendicularly to the axis of streets in both directions, using an 1.5 m high theodolite. From these data, wall view factors can be calculated to the left (WVF_{W1}) and right (WVF_{W2}) sides (*Oke*, 1981). The measuring points are not always coincident with the midpoint of the distance between buildings on both sides (*Fig. 2*). The calculation of *S* is based on *Oke's* (1988) results (for explanation of symbols see *Fig. 2*):

$$WVF_{W1} = (1 - \cos\alpha_1)/2 \qquad \text{where } \alpha_1 = \tan^{-1}(H_1/W_1), \tag{1}$$

$$WVF_{W2} = (1 - \cos\alpha_2)/2 \qquad \text{where } \alpha_2 = \tan^{-1}(H_2/W_2), \tag{2}$$

$$S = 1 - (WVF_{W1} + WVF_{W2}). \tag{3}$$

In order to determine *S* values, the same long canyons (measuring routes) were used as for temperature sampling. 532 points were surveyed by theodolite, and the values of *S* were also averaged by cells. In line with the temperature sampling, the distance between the points was 125 m on average. Angle measurements taken higher within a canyon (1.5 m) excluded more of the terrain (non-sky) and resulted in an over-estimate of *S* after the calculation. This effect is more pronounced in canyons with low *H/W* ratios (*Grimmond et al.*, 2001). Due to technical difficulties, we did not have any measurement points at the intersections of roads, so the calculated *S* values are probably a bit smaller than the real ones. Furthermore, if there were parks, forests, or water surface in a particular direction, we assigned 0° as an angle value, because it is difficult to determine *S* values modified by the vegetation, and the results are not unambiguous (*Yamashita et al.*, 1986).

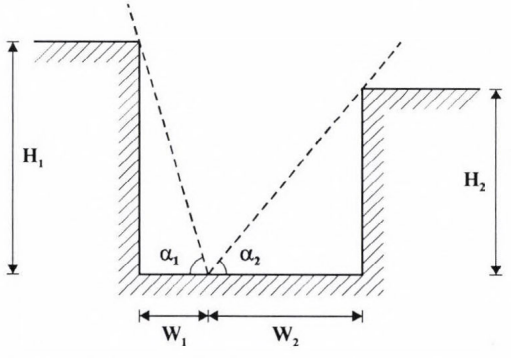

Fig. 2. Geometry of a non-symmetric canyon flanked by buildings with a measuring point not at the centre of the floor (modified after *Oke*, 1988).

While earlier investigations were limited to the centre or only some parts of the cities and used far smaller numbers of measurements (*Oke*, 1981, 1988; *Johnson*, 1985; *Yamashita et al.*, 1986; *Park*, 1987; *Eliasson*, 1996; *Grimmond et al.*, 2001), the obtained data set represents almost the total urban area.

3.5 Building height

Since some areas with different land-use features can produce almost equal *S* data (narrow street with low buildings versus broad street with high buildings), *S* values alone do not describe sufficiently the vertical geometry of cities. It is important to have quantitative information on the vertical size of a canyon, because it plays significant role in the energy budget.

To determine the vertical dimension of a canyon, we applied a combined procedure. The above mentioned elevation angles (α_1 and α_2) are available at each point. If we have the distances to the walls from the measuring point (W_1 and W_2, see *Fig. 2*), there is a simple formula to calculate wall heights (H_1 and H_2), taking the instrument height of 1.5 m into account:

$$H_1 = \tan \alpha_1 \, W_1 + 1.5 \text{ m}, \tag{4}$$

$$H_2 = \tan \alpha_2 \, W_2 + 1.5 \text{ m}. \tag{5}$$

The width of the streets was determined by means of aerial photographs concerning any part of the street. After digitizing these images, we made an orthophoto of Szeged using the Ortho Base tool of the ERDAS IMAGINE GIS software, and marked the measurement points. This orthophoto is already suitable to determine distances of the walls (W_1 and W_2) from the measurement points. As the aerial photographs do not cover completely the area of the study, these distances are not available for six and four cells in the southern and western parts of Szeged, respectively.

3.6 The applied statistical model

In order to assess the extent of the relationships between the mean maximum UHI intensity (ΔT) and various urban surface factors, multiple correlation and regression analyses were applied. Some examples of the modeled variables and employed variable parameters of earlier studies are in *Table 1*.

In the course of determination of model equations we used ΔT as predictant (dependent variable) in both seasons and the afore-mentioned parameters as predictors: ratios of built-up surface (B) and water surface (W) as a percentage, mean sky view factor (S), mean building height (H) in m by cells. Searching for statistical relationships, we have to take into account that our parameters are variables (spatially) and constants (temporally) at the same time. Since these parameters change rapidly with the increasing distance from the city center, we applied the exponentially distance-weighted spatial means of the mentioned land-use parameters for our model. The distance scale of the weight should be derived from the transport scale of the heat in the urban canopy. Our statistical model determined this scale from the measured parameter values. A set of predictors concerning all four basic urban parameters were originated as areal extensions and grouped in the following way:

Group 1: parameter values (S, H, B, W) in the cell with $\Delta i^2 + \Delta j^2 = 0$.

Group 2: mean parameter values ($S1$, $H1$, $B1$, $W1$) of all cells with $0 < \Delta i^2 + \Delta j^2 < 2^2$.

Group 3: mean parameter values ($S2$, $H2$, $B2$, $W2$) of all cells with $2^2 < \Delta i^2 + \Delta j^2 < 4^2$.

Here i and j are cell indices in the two dimensions, while Δi and Δj are the differences of cell indices with respect to a given cell. These zones cover the entire investigated model area of Szeged.

Table 1. Survey of some studies using statistical models for prediction of UHI (extended after *Unger et al.*, 2000)

Predicted variable	Employed parameters	Reference
UHI intensity	Wind speed, cloudiness	*Sundborg* (1950)
UHI intensity	Population, wind speed	*Oke* (1973)
Max. UHI intensity	Population	
UHI intensity	Wind speed, cloudiness, atmospheric stability, traffic flow, energy consumption, temperature	*Nkemdirim* (1978)
UHI intensity at four different air levels	Lapse rate, wind speed, ratio of lapse rate to wind speed	*Nkemdirim* (1980)
UHI intensity	Wind speed, land-use type ratios	*Park* (1986)
Max. UHI intensity	Impermeable surface, population	
UHI intensity	Wind speed, cloudiness, temperature, humidity mixing ratio	*Goldreich* (1992)
UHI intensity	Wind speed, cloudiness, air pressure	*Moreno-Garcia* (1994)
Surface UHI intensity	Solar radiation, wind speed, cloudiness	*Chow et al.* (1994)
UHI intensity	Built-up area, height, wind speed, time, temperature amplitude	*Kuttler et al.* (1996)
UHI intensity for T_{avg}, T_{max}, T_{min}	NDVI, surface temperature (satellite-based)	*Gallo* and *Owen* (1999)
UHI intensity	Distance from the city centre, built-up ratio	*Unger et al.* (2000)
UHI intensity	Wind speed, cloudiness	*Morris et al.* (2001)

With these areal extensions we have 12 predictors to construct the linear statistical model. However, there could be some multi-colinearity among these parameters. In order to eliminate these multi-colinearities, the set of parameters have to be selected. Using the cross-correlation matrix of these predictors we can find the highest correlation coefficients, which means strong connections among them. To avoid the unreasonable reduction of the number of predictors, only the parameter with maximum absolute mean of its correlation coefficients was taken out of each group.

The method for the construction of model equations is the stepwise multiple linear regression. The applied implementation of this procedure is part of the SPSS 9 statistical software. A comprehensive discussion of the mathematical background of this method is found in *Miller* (2002). Predictors were entered or removed from the model depending on the significance of the F value of 0.01 and 0.05, respectively. Since there is a well noticeable difference between the magnitudes of ΔT fields in these seasons, under these conditions two linear statistical model equations were determined: one for the heating and one for the non-heating season.

3.7 Cross-section investigation

A small but representative part of the original area of the study (altogether 10 cells) is examined seasonally in detail. This is an overlapping part between the northern and southern sectors (*Fig. 1*), namely a cross-section in the urban area, which consists of cells stretching from the rural area (cell 1) to the city core (cell 10) with a distance of 4.5 km.

The profiles of the UHI intensity along the cross-section were investigated by comparison of absolute and normalized seasonal means taking land-use and climatological features into consideration. The normalized values by cells are the ratios of the absolute means of a given cell and cell 10 (where ΔT is the highest in all seasons). Since meteorological conditions (first of all wind speed and cloudiness) influence the absolute values (in °C) of the UHI intensity (e.g., *Landsberg*, 1981; *Park*, 1986; *Yagüe et al.*, 1991; *Unger*, 1996), the seasonal comparison of spatial variation of ΔT is more effective using normalized values. Namely, the profile of the normalized seasonal mean UHI intensity is expected to be independent of the prevailing weather conditions in the studied period; nevertheless, it is expected to be dependent on the surface factors (e.g., land-use features, distance from the city centre, etc.).

4. Results and discussion

4.1 Spatial characteristics of the urban parameters and UHI

The spatial distribution of the built-up ratio in the city has almost a concentric shape decreasing from the central areas to outwards (*Fig. 3a*). The densely built-up areas are concentrated in the middle and north-eastern parts of the city with maximum values more than 96%. River Tisza with its environment has a low built-up ratio and, of course, a high water surface ratio which can be clearly recognized with its east-to-south curve (*Fig. 3b*). Apart from this, the

extension of water surfaces is negligible, except for some small and shallow recreational lakes in the western part of the city.

Due to the significant variability of the building height and width of the streets, the sky view factor pattern is very complicated (*Fig. 3c*). This field does not form a circular structure and its extreme values are not located only in the centre. There are three parts of the city where S is low (with values of lower than 0.8), and in the centre it is lower than 0.7. The highest buildings are concentrated in the north-eastern part of the city with maximum values of about 20 m (*Fig. 3d*). There is an other area in the southern central region, where the buildings are higher than 15 m. Generally, the average building height is more than 10 m in the studied area.

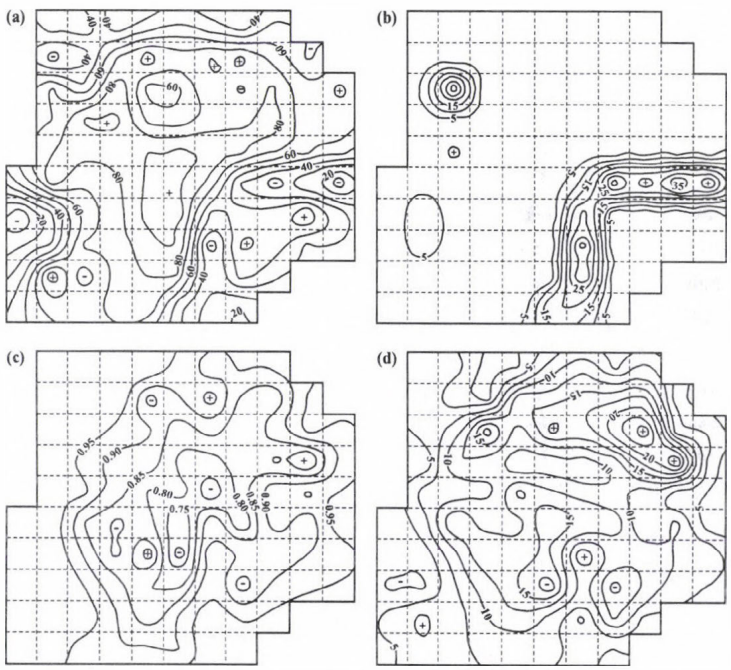

Fig. 3. Spatial distribution of (*a*) the ratio of the built-up area, (*b*) the ratio of the water surface to the total area (in percent), (*c*) the average sky view factor values and (*d*) the average building heights (in m) by cells in Szeged.

In the non-heating season (*Fig. 4a*), the greatest mean UHI intensity (3.18 C) is found in the central cell, and the ΔT of higher than 2 C – indicating significant thermal modification caused by urbanization – covers about 37% of the investigated area. In the heating season (*Fig. 4b*), the highest value of the

UHI intensity (2.12°C) occurs in the central cell, too, but the area of considerable differences (>2°C) covers only about 2% of the total area (*Unger et al.*, 2000).

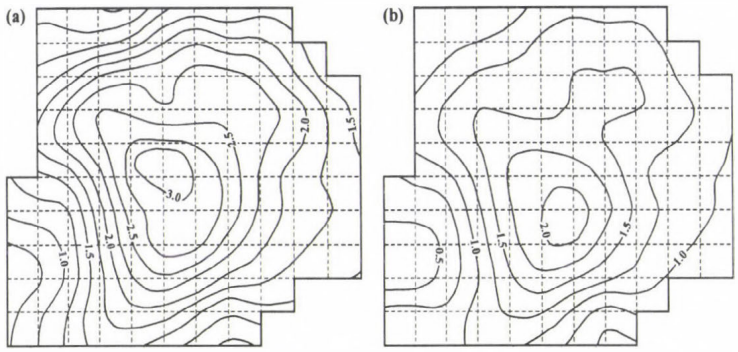

Fig. 4. Spatial distribution of the measured mean maximum UHI intensity (°C) during (*a*) the non-heating season (April 16 – October 15: 26 measurements) and (*b*) the heating season (October 16 – April 15: 22 measurements) in Szeged.

The most obvious common features of the UHI patterns are that the isotherms show almost concentric shapes in both seasons (*Fig. 4*). A deviation from this shape occurs in the north-eastern part of the city, where the isotherms stretch towards the suburbs. This anomaly can be explained by the effect of the large housing estates with high concrete buildings located mainly in the north-eastern part of the city with a built-up ratio higher than 75% (*Fig. 3a*), a sky view factor less than 0.85 (*Fig. 3c*), and a building height more than 15 m (*Fig. 3d*). The second irregularity is caused by the cooling influence of River Tisza, because along the river the isotherms are a bit drawn back towards the centre. The third area of anomaly can be found in the western part of the city, where the surface geometry changes abruptly along a westbound transect (which starts at the centre). This region is characterized by S values higher than 0.95, building heights lower than 7 m, and built-up ratio of about 25%.

The seasonal differences in the spatial distribution of ΔT (in °C) may be formed rather as a consequence of different weather characteristics of the two seasons than as a consequence of heating or non-heating of dwellings. In the Szeged region the climate conditions in winter, conducing to the formation of UHI, are less common (*Table 2*). Thus, in the warmer (non-heating) season, the role of the weather conditions (stronger solar radiation, more frequent clear sky, and weak wind) and the reduced latent heat transport, due to the more impermeable and guttered urban terrain, is more pronounced in the

development of UHI than the anthropogenic heat emission by heating in the colder season (*Unger et al.*, 2000).

Table 2. Monthly and seasonal means of the selected meteorological parameters in Szeged (March 1999 – February 2000)

Period	M	A	M	J	J	A	S	O	N	D	J	F	Spr.	Sum.	Aut.	Win.
Wind speed ($m\ s^{-1}$)	3.5	3.5	2.6	2.5	2.6	2.1	2.7	2.9	2.6	3.4	3.5	3.4	3.2	2.4	2.7	3.4
Cloudiness (okta)	4.7	4.9	4.3	4.6	3.8	3.6	3.6	4.5	5.9	5.6	6.1	3.7	4.6	4.0	4.7	5.1

4.2 Statistical model equations

Table 3 contains the cross-correlation matrix of the predictors and maximum absolute means of the correlation coefficients by lines. As a result of the selection procedure to reduce the multi-colinearities, three parameters (*S*, *H*1, and *S*2) were taken out of the original parameter-set. Thus, for the construction of the model equations, nine predictors remained.

Table 3. Cross-correlation matrix of the parameters and absolute means of the correlation coefficients by lines. Parameters are taken out of the models, and their absolute means are marked with bold setting (see Section 3.3–3.6 for explanation)

Parameter	B	S	W	H	B1	S1	W1	H1	B2	S2	H2	W2	Abs. mean
B	-	-0.50	-0.48	0.52	0.62	-0.50	-0.24	0.45	0.11	-0.12	0.01	-0.12	0.33
S	-0.50	-	0.13	-0.72	-0.52	0.64	0.09	-0.55	-0.05	0.41	-0.33	0.02	**0.36**
W	-0.48	0.13	-	-0.16	-0.13	0.02	0.29	-0.10	0.04	-0.22	0.18	0.16	0.17
H	0.52	-0.72	-0.16	-	0.43	-0.50	-0.16	0.57	-0.01	-0.42	0.23	-0.11	0.34
B1	0.62	-0.52	-0.13	0.43	-	-0.64	-0.49	0.57	0.15	-0.14	0.06	-0.21	0.36
S1	-0.50	0.64	0.02	-0.50	-0.64	-	0.04	-0.84	-0.04	0.56	-0.49	0.08	0.39
W1	-0.24	0.09	0.29	-0.16	-0.49	-0.04	-	-0.14	-0.08	-0.27	0.17	0.24	0.20
H1	0.45	-0.55	-0.10	0.57	0.57	-0.84	-0.14	-	-0.03	-0.63	0.48	-0.08	**0.40**
B2	0.11	-0.05	0.04	-0.01	0.15	-0.04	-0.08	-0.03	-	-0.10	0.21	0.02	0.08
S2	-0.12	0.41	-0.22	-0.42	-0.14	0.56	-0.27	-0.63	-0.10	-	-0.85	-0.10	**0.35**
H2	0.01	-0.33	0.18	0.23	0.06	-0.49	0.17	0.48	0.21	-0.85	-	0.13	0.28
W2	-0.12	0.02	0.16	0.23	-0.21	0.08	0.24	-0.08	0.02	-0.10	0.13	-	0.12

In both seasons the order of significance of the applied parameters is the same, but in the heating season the role of them is more pronounced than in the non-heating season. The model equations have four predictors, among them the *S*1 predictor is the most important, but *H* and *B*1 factors also play important role in both seasons (*Table 4*).

Table 4. Values of the stepwise correlation of mean maximum UHI intensity (ΔT) and urban surface parameters, and their significance levels in the studied periods in Szeged (n = 97) (see Section 3.3–3.6 for explanation)

Period	Parameter entered	Multiple |r|	Multiple r^2	Δr^2	Significance level (%)
April 16 - October 15 (non-heating season)	S1	0.806	0.649	0.000	0.1
	S1, H	0.845	0.714	0.065	0.1
	S1, H, B1	0.863	0.744	0.030	0.1
	S1, H, B1, W1	0.902	0.814	0.070	0.1
October 16 - April 15 (heating season)	S1	0.791	0.626	0.000	0.1
	S1, H	0.834	0.696	0.070	0.1
	S1, H, B1	0.852	0.726	0.030	0.1
	S1, H, B1, W1	0.873	0.762	0.036	0.1

The four-variable models for the non-heating (*nh*) and heating (*h*) seasons indicate strong linear relation between the mean maximum UHI intensity and the applied land-use parameters (*Table 4*). The model equations for ΔT_{nh} and ΔT_h (in °C) are the next (*Table 5*):

$$\Delta T_{nh} = -4.291S1 + 0.035H + 0.023B1 + 0.042W1 + 3.824, \quad (6)$$

$$\Delta T_h = -3.242S1 + 0.025H + 0.014B1 + 0.021W1 + 3.036. \quad (7)$$

The absolute values of the multiple correlation coefficients (r) between ΔT and the studied parameters are 0.902 and 0.873 in the non-heating and heating seasons; both are significant at 0.1% level. This means that with these four parameters we are able to explain 81.4% and 76.2% of the above mentioned relationships in the studied periods (*Table 4*). The standard errors of the estimates are 0.272 and 0.218 in the non-heating and heating half year, respectively.

We used these two model equations ((6) and (7)) to determine the spatial distribution of ΔT patterns in the studied area (*Fig. 5*). There is a considerable similarity between the measured and predicted UHI intensity fields in both seasons, namely, they have the same irregularities, however, some differences can be detected (*Fig. 4* and *Fig. 5*).

Table 5. Values of significance, coefficients, and standard errors of the applied urban surface parameters of the models in the studied periods in Szeged (n = 97) (see Section 3.3–3.6 for explanation)

Period	Parameter	Significance	Coefficient	Standard error
April 16 – October 15 (non-heating season)	S1	0.000	**-4.291**	0.787
	H	0.000	**0.035**	0.006
	B1	0.000	**0.023**	0.003
	W1	0.000	**0.042**	0.007
	Const.	0.000	**3.824**	0.897
October 16 – April 15 (heating season)	S1	0.000	**-3.242**	0.631
	H	0.017	**-0.025**	0.005
	B1	0.006	**0.014**	0.003
	W1	0.022	**0.021**	0.006
	Const.	0.000	**3.036**	0.718

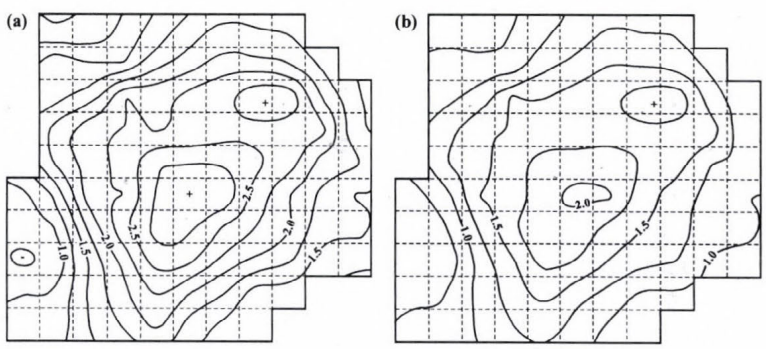

Fig. 5. Spatial distribution of the predicted mean max. UHI intensity (°C) during the (*a*) non-heating season and (*b*) the heating season in Szeged.

We compared the results of the model to an independent UHI intensity data set measured during the non-heating half year in 2002. The studied area and the mobile sampling method were the same as in the earlier cases, except that we used two cars to take temperature measurements at the same time in the two sectors, altogether 18 times. According to *Fig. 6a*, the measured independent UHI intensity pattern is similar to the one mentioned above (*Fig. 5a*), though the largest ΔT value is smaller by about 0.5°C. After that we calculated the spatial distribution of the difference between the predicted and measured independent UHI intensities (*Fig. 6b*). We can find only two small areas where the absolute UHI intensity anomaly is between 0.4°C and 0.6°C.

In the north-eastern part of the city, the predicted values are lower than the measured ones (negative anomaly). At the western border of the investigated area the predicted values are higher than the measured ones (positive anomaly). However, these areas occupy only a minor part of the area of the study (about 3.9 cells, 1 km^2, 4% of the total area). The areas characterized by the differences lower than 0.2°C are significantly larger, covering altogether 73 cells (about 18,2 km^2, 75%).

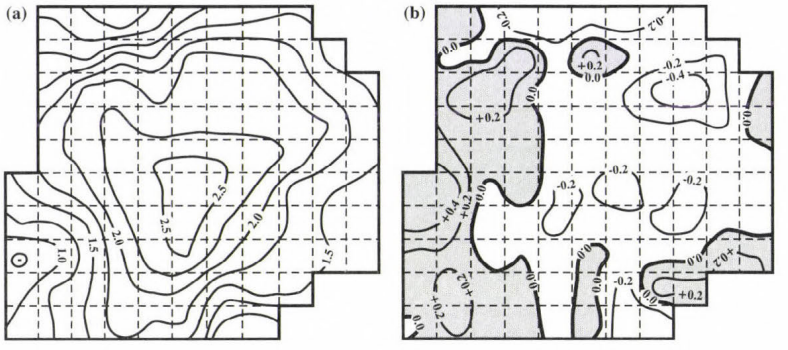

Fig. 6. (*a*) Spatial distribution of the measured mean max. UHI intensity (°C) during the independent non-heating season in 2002 and (*b*) spatial distribution of the difference of measured and predicted mean max. UHI intensity (°C) during the same season in Szeged.

It can be established that our model described the spatial distribution of the real UHI intensity field in the investigated area rather correctly. On the basis of our results, we may apply this model-construction procedure to predict the ΔT for other cities of different size and even non-concentric shape.

4.3 Cross-section profiles of UHI by seasons

Table 6 contains the areal ratios (%) of the main land-use types by cells along the selected cross-section. The largest built-up density (more than 90%) can be found around the centre (see cells 9 and 10 in *Fig. 1*), but the variation from the urban edge to the core is not uniform. The proportion of the water surface is rather negligible.

According to *Fig. 7a,* the profiles in every season show a marked increase from a rural level after reaching the edge of built-up areas (cell 3, see *Table 6*), and the highest values are in the city centre (cell 10). The absolute values of the seasonal profiles are almost the same in every cell, with the exception of winter. The values of the winter profile (with the largest seasonal

mean UHI intensity of 1.44°C) do not reach even the half of the values of other seasons. Because of the low winter values, the mean annual profile is a bit moderate compared to the ones of the first three seasons (the largest ΔT is 2.58°C).

Table 6. Land-use types by cells along the urban cross-section in Szeged

Land-use type (%)	Cell number									
	1	**2**	**3**	**4**	**5**	**6**	**7**	**8**	**9**	**10**
Built-up	0	0	18.9	70.4	54.2	85.6	71.7	77.8	91.4	90.5
Open	100	100	81.1	23.5	45.3	11.1	28.3	22.2	8.6	9.1
Water	0	0	0	6.1	0.5	3.3	0	0	0	0.4

Using normalized values, the differences among the seasonal profiles tend to disappear (*Fig. 7b*). These patterns follow remarkably well the general cross-section profile of the typical UHI described by *Oke* (1987): the 'cliff' is a steep temperature gradient at the rural/urban boundary, and much of the rest of the urban area appears as a 'plateau' of warm air with a steady but weaker horizontal gradient of increasing temperature towards the city centre. The urban core shows a final 'peak', where the largest temperature difference is observed (*Fig. 7c*).

In Szeged, the normalized ΔT values varied together along the cross-section with the largest deviation of only 0.13, in all seasons and in the whole one-year period (*Fig. 7b*). The 'cliff' with the large temperature gradient is located between cells 2 and 4 (the distance is 1 km). The profile shows a 1.5 km long thermal 'plateau' which is characterized by a very low temperature increment through its four cells (from 4 to 7). Then there is a second, very steep 'cliff' between the cells 7 and 8 (0.5 km), which indicates the onset of the 'peak' region. The areal extent of the largest values are rather wide (three cells, 1 km), so the steepness at the 'peak' value is relatively less sharp. This is explicable by the extent and homogeneity of the central urban part, which is dominated by 3–5 storey buildings built around the turn of the 19th and 20th centuries after the so called 'Great Flood' in 1879, which destroyed the city.

The seasonal variation of the urban temperature anomaly along the cross-section is attributed mainly to differences in weather conditions (*Table 2*). Winter months have the highest wind speed and cloudiness: at this time the UHI intensity is the weakest. In summer, when the above mentioned parameters have the smallest values, the extent of ΔT is not the largest in every point along the cross-section: it is slightly under or over the ΔT values in spring and autumn. These facts suggests that the effects of the climatological

parameters are fairly complex, and the investigation of their influence on the UHI cannot be restricted to only two, although important, parameters.

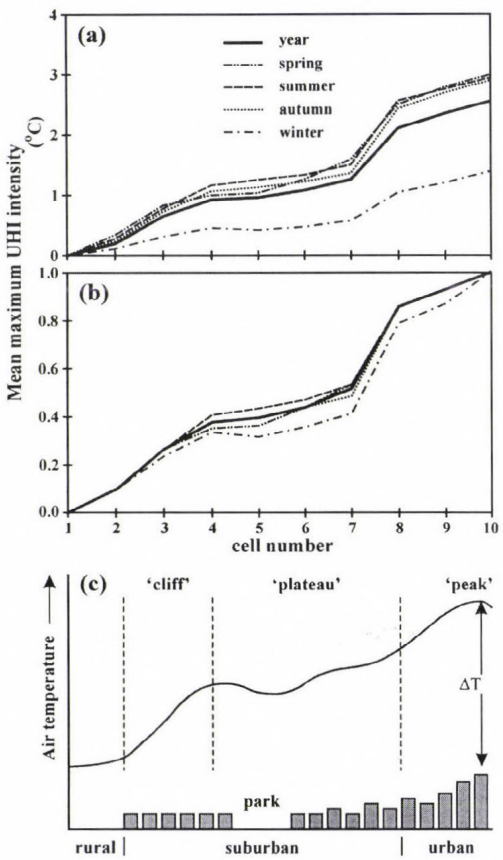

Fig. 7. Seasonal and annual profiles of (*a*) the absolute and (*b*) the normalized mean maximum UHI intensity across Szeged. (*c*) Generalized cross-section of the typical UHI after sunset (modified after *Oke*, 1987).

The use of the normalized values proved that the form of seasonal mean UHI profile depends only on surface factors. Among these factors, the built-up ratio may not be the most important one, because the steady, but not uniform increment of temperature towards the city core does not follow exactly the built-up density variation by cells (*Table 6*). However, an another parameter, however, the distance from the city centre seems to be more dominant in this general increasing tendency of urban temperature (*Unger et al.*, 2000).

5. Conclusions

In this paper the spatial and temporal features of the UHI effect was investigated in Szeged, Hungary. The following conclusions can be drawn from the analysis presented:

- The heat island phenomenon always appeared in the studied area, even though the UHI intensity changed during the year, as a consequence of the prevailing weather conditions, which vary by seasons in the temperate climatic region.
- The results on the seasonal spatial distribution of mean UHI indicate that:
  (i) The spatial patterns of the UHI intensity have almost concentric shapes with the values decreasing from the central areas towards the outskirts. The anomalies are caused by the alterations in the urban surface factors.
  (ii) There are significant differences in the magnitudes of the seasonal patterns. The area of the mean UHI intensity higher than 2°C is far larger in the non-heating than in the heating season.
- The statistical estimation of the spatial distribution of mean UHI intensity by the aid of surface parameters indicates that:
  (i) On the basis of the statistical analysis there is a strong linear relationship between the mean UHI intensity and the studied urban parameters, such as sky view factor, building height, built-up ratio, water surface ratio, and their areal extensions in both seasons.
  (ii) Generally, our model described the spatial distribution of the real UHI intensity field in the area of the study rather correctly, because the areas characterized by the differences lower than 0.2°C cover the larger parts of the city (75%). Nevertheless, there are small differences between the predicted and measured UHI fields, which are caused by some possible errors in the temperature samplings, the low number of studied parameters, and the considerable irregularities of the surface geometry.
  (iii) This procedure, used to predict the UHI intensity, may be applicable for other cities of different size and even non-concentric shape, but for the true validation it is necessary to have complete databases of measured intensities for those cities.
- The profile of mean UHI and its seasonal variation along a cross-section indicates that:
  (i) The seasonal profiles follow remarkably well the general cross-section of the typical UHI.

(ii) The role of cloudiness and wind speed on the seasonal variation of the UHI is clearly recognized throughout the one-year period.

(iii) The usefulness of the normalized values in the investigaton of the cross-section temperature distribution has been proved. It came to light, that the shape of the seasonal mean UHI profile is independent of the seasonal weather conditions, and it is determined mainly by the surface factors.

- Consequently, our preliminary results prove that the statistical approach on estimation of the UHI intensity in Szeged is promising. We are planning to extend this project by modeling urban thermal patterns as they are affected by weather conditions with a time lag. We intend to employ the same parameters used in this study, as well as additional urban and meteorological parameters, to predict the magnitude and spatial distribution of the UHI intensity on the days characterized by any kind of weather conditions (apart from precipitation), at any time of the year, without having recourse to extra mobile measurements. Although, adding meteorological predictors increase the complexity of the model, it may give us a useful tool for the prediction of the temperature field for several hours in advance.

Acknowledgements—The authors wish to give special thanks to *P. Purnhauser, E. Robotka,* and *Z. Zboray* who took part in the measurement campaigns and data pre-processing, and to the reviewers for their helpful suggestions. This research was supported by the grant of the Hungarian Scientific Research Fund (OTKA T/034161). The work of the first author was also supported by the Széchenyi István Grant of the Ministry of Education.

References

Bärring, L., Mattsson, J.O., and *Lindqvist, S.*, 1985: Canyon geometry, street temperatures and urban heat island in Malmö, Sweden. *Int. J. Climatol. 5*, 433-444.

Chow, S.D., Zheng, J., and *Wu, L.*, 1994: Solar radiation and surface temperature in Shangai City and their relation to urban heat island intensity. *Atmos. Environ. 28*, 2119-2127.

Conrads, L.A. and *van der Hage, J.C.H.*, 1971: A new method of air-temperature measurement in urban climatological studies. *Atmos. Environ. 5*, 629-635.

Eliasson, I., 1996: Urban nocturnal temperatures, street geometry and land use. *Atmos. Environ. 30*, 379-392.

Gallo, K.P. and *Owen, T.W.*, 1999: Satellite-based adjusments for the urban heat island temperature bias. *J. Appl. Meteorol. 38*, 806-813.

Golany, G.S., 1996: Urban design morphology and thermal performance. *Atmos. Environ. 30*, 455-465.

Goldreich, Y., 1992: Urban climate studies in Johannesburg, a sub-tropical city located on a ridge – A review. *Atmos. Environ. 26B*, 407-420.

Grimmond, C.S.B. and *Oke, T.R.*, 1991: An evapotranspiration-interception model for urban areas. *Water Resour. Res. 27*, 1739-1755.

Grimmond, C.S.B., Cleugh, H.A., and *Oke, T.R.*, 1991: An objective urban heat storage model and its comparison with other schemes. *Atmos. Environ. 25B*, 311-326.

Grimmond, C.S.B., Potter, S.K., Zutter, H.N., and *Souch, C.*, 2001: Rapid methods of estimate sky-view factors applied to urban areas. *Int. J. Climatol. 21*, 903-913.

Johnson, D.B., 1985: Urban modification of diurnal temperature cycles in Birmingham. *J. Climatol. 5*, 221-225.

Johnson, G.T., Oke, T.R., Lyons, T.J., Steyn, D.G., Watson, I.D., and *Voogt, J.A.*, 1991: Simulation of surface urban heat islands under 'ideal' conditions at night, I: Theory and tests against field data. *Bound.-Lay. Meteorol. 56*, 275-294.

Klysik, K. and *Fortuniak, K.*, 1999: Temporal and spatial characteristics of the urban heat island of Lódz, Poland. *Atmos. Environ. 33*, 3885-3895.

Kuttler, W., Barlag, A.-B., and *Roßmann, F.*, 1996: Study of the thermal structure of a town in a narrow valley. *Atmos. Environ. 30*, 365-378.

Landsberg, H.E., 1981: *The Urban Climate*. Academic Press, New York.

Matzarakis, A., Beckröge, W., and *Mayer, H.*, 1998: Future perspectives in applied urban climatology. *Proceed. The Second Japanese-German Meeting*. RCUSS, Kobe University, 109-122.

Miller, A.J., 2002: *Subset Selection in Regression*. Chapman&Hall/CRC, Boca Raton.

Moreno-Garcia, M.C., 1994: Intensity and form of the urban heat island in Barcelona. *Int. J. Climatol. 14*, 705-710.

Morris, C.J.G., Simmonds, I., and *Plummer, N.*, 2001: Quantification of the influences of wind and cloud on the nocturnal urban heat island of a large city. *J. Appl. Meteorol. 40*, 169-182.

Myrup, L.O., McGinn, C.E., and *Flocchini, R.G.*, 1993: An analysis of microclimatic variation in a suburban environment. *Atmos. Environ. 27B*, 129-156.

Nkemdirim, L.C., 1978: Variability of temperature fields in Calgary, Alberta. *Atmos. Environ. 12*, 809-822.

Nkemdirim, L.C., 1980: A test of lapse rate/wind speed model for estimating heat island magnitude in an urban airshed. *J. Appl. Meteorol. 19*, 748-756.

Oke, T.R., 1973: City size and the urban heat island. *Atmos. Environ. 7*, 769-779.

Oke, T.R., 1976: The distinction between canopy and boundary layer urban heat islands. *Atmosphere 14*, 268-277.

Oke, T.R., 1981: Canyon geometry and the nocturnal urban heat island: comparison of scale model and field observations. *J. Climatol. 1*, 237-254.

Oke, T.R., 1987: *Boundary Layer Climates*. Routledge. London and New York, 405 pp.

Oke, T.R., 1988: Street design and urban canopy layer climate. *Energ. Buildings 11*, 103-113.

Oke, T.R. and *Fuggle, R.F.*, 1972: Comparison of urban/rural counter and net radiation at night. *Bound.-Lay. Meteorol. 2*, 290-308.

Oke, T.R. and *Maxwell, G.B.*, 1975: Urban heat island dinamics in Montreal and Vancouver. *Atmos. Environ. 9*, 191-200.

Outcalt, S.I., 1972: A synthetic analysis of seasonal influences in the effects of land use on the urban thermal regime. *Arch. Meteor. Geophy. B 20*, 253-260.

Park, H.-S., 1986: Features of the heat island in Seoul and its surrounding cities. *Atmos. Environ. 20*, 1859-1866.

Park, H.-S., 1987: Variations in the urban heat island intensity affected by geographical environments. *Environmental Research Center Papers 11*. The University of Tsukuba, Ibaraki, Japan, 79 pp.

Ruffieux, D., 1995: Winter surface energy budget in Denver, Colorado. *Atmos. Environ. 29*, 1579-1587.

Sundborg, A., 1950: Local climatological studies of the temperature conditions in an urban area. *Tellus 2*, 222-232.

Tapper, P.D., Tyson, P.D., Owens, I.F., and *Hastie, W.J.*, 1981: Modeling the winter urban heat island over Christchurch. *J. Appl. Meteorol. 20*, 365-367.

Unger, J., 1996: Heat island intensity with different meteorological conditions in a medium-sized town: Szeged, Hungary. *Theor. Appl. Climatol. 54*, 147-151.

Unger, J., 1999: Urban-rural air humidity diferences in Szeged, Hungary. *Int. J. Climatol. 19*, 1509-1515.

Unger, J., Bottyán, Z., Sümeghy, Z., and *Gulyás, A.*, 2000: Urban heat island development affected by urban surface factors. *Időjárás 104*, 253-268.

Unger, J., Sümeghy, Z., and *Zoboki, J.*, 2001: Temperature cross-section features in an urban area. *Atmos. Res. 58*, 117-127.

Voogt, J.A. and *Oke, T.R.*, 1991: Validation of an urban canyon radiation model for nocturnal long-wave radiative fluxes. *Bound.-Lay. Meteorol. 54*, 347-361.

Voogt, J.A. and *Oke, T.R.*, 1997: Complete urban surface temperatures. *J. Appl. Meteorol. 36*, 1117-1132.

Voogt, J.A. and *Grimmond, C.S.B.*, 2000: Modeling surface sensible heat flux using surface radiative temperatures in a simple urban area. *J. Appl. Meteorol. 39*, 1679–1699.

Yagüe, C., Zurita, E., and *Martinez, A.*, 1991: Statistical analysis of the Madrid urban heat island. *Atmos. Environ. 25B*, 327-332.

Yamashita, S., 1996: Detailed structure of heat island phenomena from moving observations from electric tram-cars in metropolitan Tokyo. *Atmos. Environ. 30*, 429-435.

Yamashita, S., Sekine, K., Shoda, M., Yamashita, K., and *Hara, Y.*, 1986: On the relationships between heat island and sky view factor in the cities of Tama River Basin, Japan. *Atmos. Environ. 20*, 681-686.

IDŐJÁRÁS

Quarterly Journal of the Hungarian Meteorological Service
Vol. 108, No. 3, July–September 2004, pp. 195–208

Radiation maps of Hungary

Anikó Rimóczi-Paál

Hungarian Meteorological Service
P.O. Box 39, H-1675 Budapest, Hungary

(Manuscript received June 18, 2003; in final form August 4, 2003)

Abstract—The meteorologist always considered the mapping of solar energy reaching the surface as main object to supply useful information for engineers and scientists working in the agriculture, designing buildings, and other spheres of the economy, where the solar energy plays an important role. In Hungary, the first radiation maps were already constructed in the time of the publication of the first radiation maps in the world. First, in the present paper, traditional radiation maps of Hungary are reviewed.

Meteorological satellite data represent proper input information for estimating surface radiation balance at high spatial resolution. In this study a method of mapping the radiation balance components, i.e., global radiation, downward longwave radiation, shortwave and longwave radiation balance, and net radiation of the surface, is presented and illustrated for the territory of Hungary (93,000 km^2). The radiation balance components were calculated by a relatively simple model developed at the Satellite Research Laboratory of the Hungarian Meteorological Service. Digital images from the METEOSAT satellite and radiosonde observations for the period of 1992–1996 were used for this purpose. The methodology was validated for all components by using 10×10 km^2 area around the BSRN (Baseline Surface Radiation Network) station at Budapest-Lőrinc. Stratified sampling, according to a macrosynoptic classification, is applied before processing the monthly radiation maps to make the 5-year satellite samples more representative for the 1961–1990 climate period. For example, maps of global radiation in July and net radiation in January are shown.

Key-words: radiation map, global radiation, net radiation, satellite data, solar energy.

1. Introduction

The first radiation maps of Hungary (*Dobosi* and *Takács*, 1959) were already constructed simultaneously with the publication of the first radiation maps in developed countries. From the measurements of the Robitzsch and later of the thermo-electrical instruments new and new radiation maps were derived in

Hungary. The traditional radiation network did not make possible to derive radiation maps with a good spatial resolution. Meteorological satellites have given a new opportunity for estimation of much more detailed radiation maps than those constructed by using only traditional surface radiation measurements, not always having long-term spatial representativity and backward quality assurance. Different methods were elaborated in the world to determine radiation maps from satellite data. Hence, a relatively simple model has been developed at Satellite Research Laboratory of the Hungarian Meteorological Service to derive components of the radiation budget with a spatial resolution of 10×10 km^2 using data of METEOSAT satellite, empirical formulae, and a radiative transfer model.

2. Traditional radiation maps of Hungary

First map of incoming solar radiation – the global radiation – for region of Hungary and for the period 1901–1950 was derived by *Dobosi* and *Takács* (1959). They calculated the global radiation by using different modified Ångström formulae for 14 regions of Hungary from sunshine duration of 45 stations. The Ångström formulae were determined from the measurements of the International Geophysical Year (1957). Spatial distribution of the global radiation in July obtained by them is shown in *Fig. 1*.

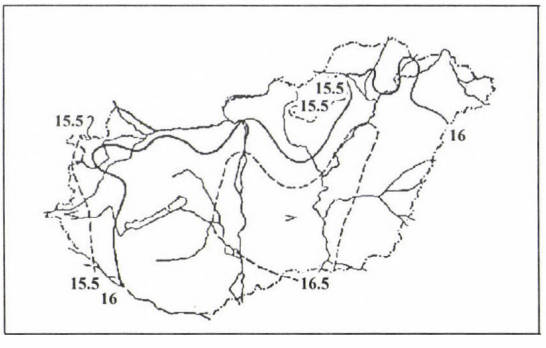

Fig. 1. Global radiation in July for the period 1901–1950 (kcal cm^{-2}) (after *Dobosi* and *Takács*, 1959).

Continuous recording of the solar irradiation of the horizontal plane began in 1936 using bimetallic pyranographs. Since that time as many as 38 radiation stations have been established in Hungary, most of them in the International

Geophysical Year (1957). Of these stations only 15 Robitzsch instruments recorded the global radiation in Hungary for at least 15 years. *Takács* (1974) published the first map of spatial distribution of the global radiation on the basis of direct radiation measurements in Hungary.

From the measurements of Robitzsch instruments the Radiation Division of the Hungarian Meteorological Service published the first measured climatological dataset of the solar radiation edited by *Major* (1976). The global radiation maps were constructed from the measurements of 13 Robitzsch instruments and by empirical formulae from the sunshine duration of maximum 33 stations. The net radiation was calculated by empirical formulae from the global radiation. To illustrate these calculations *Fig. 2* shows the spatial distribution of global radiation in July, while in *Fig. 3* spatial distribution of net radiation in January can be seen.

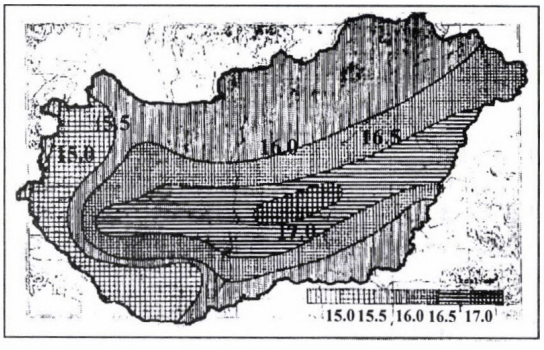

Fig. 2. Global radiation in July for the period 1958–1972 (kcal cm^{-2}) (after *Major*, 1976).

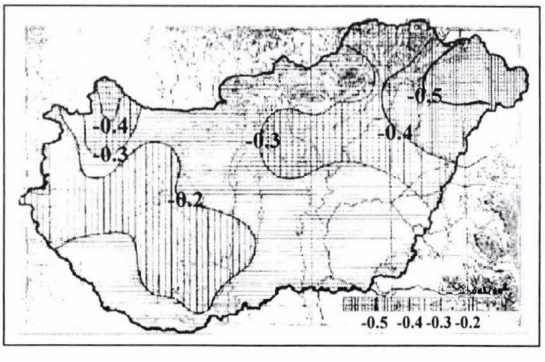

Fig. 3. Net radiation in January for the period 1958–1972 (kcal cm^{-2}) (after *Major*, 1976).

Later the Robitzsch instruments were changed to modern thermoelectric pyranometers, and 6 stations measured continuously the global radiation and one station (Budapest-Lőrinc) registered all components of the radiation balance. *Major* and *Takács* (1985) constructed 25-year global radiation maps using measurements in the period 1958–1982. *Dávid et al.* (1990) published the 30-year (1951–1980) maps of global radiation, surface albedo, short-wave radiation balance, and net radiation. These radiation maps have had the best spatial resolution before maps derived using satellite information. The region of Hungary was separated into 44 polygons providing spatial resolution approximately 80 × 80 km^2. Every polygon contained one or more stations measuring either global radiation or sunshine duration. The global radiation maps were calculated partly from surface measurements and partly from sunshine duration by using empirical formulae. Ångström formulae improved by *Dobosi* and *Takács* (1959) were also applied for the estimation of the global radiation from the sunshine duration. Maps of short-wave radiation balance and net radiation were derived from the global radiation using empirical formulae. Maps of the long-wave components of radiation balance could not be constructed because of absence of measurements. In *Fig. 4* spatial distribution of the global radiation in July, while in *Fig. 5* that of the net radiation in January can be seen after *Dávid et al.* (1990).

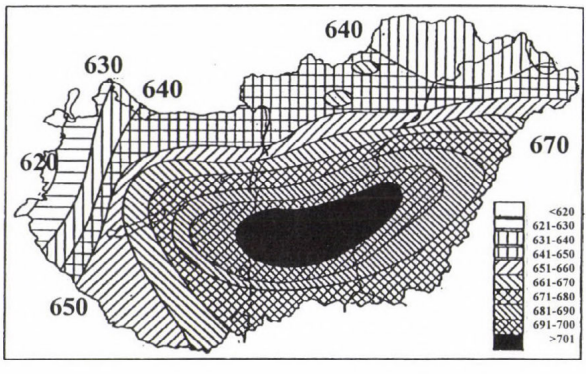

Fig. 4. Global radiation in July for the period 1951–1980 (MJ m^{-2}) (after *Dávid et al.*, 1990).

Since 1994, 13 automatic meteorological stations have been measuring the global radiation in Hungary, but only one station (Budapest-Lőrinc) measures all components of the radiation balance. Satellite Research Laboratory of the Hungarian Meteorological Service has received and archived data of METEOSAT and NOAA satellites since 1992. The new information gave good

opportunity to map both short-wave and long-wave components of the radiation balance with a very good spatial resolution.

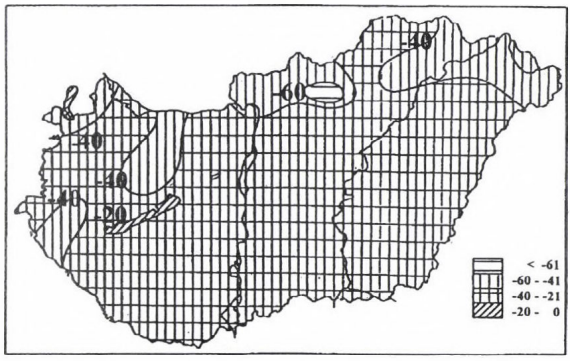

Fig. 5. Net radiation in January for the period 1951–1980 (MJ m^{-2}) (after *Dávid et al.*, 1990).

3. Methodology

Schmetz (1989), *Sellers et al.* (1990), and *Eymard* and *Taconet* (1995) reviewed a large number of methods using satellite data developed in the last 30 years to estimate surface radiation budget components. The algorithms can be classified as empirical and physical methods, and into a combined use of satellite data and numerical weather forecast models (*Brisson et al.*, 1994). The empirical methods are based on regression between co-located simultaneous satellite radiances and measured insolation at surface (*Fritz* and *Rao*, 1967; *Tarpley*, 1979; *Klink* and *Dollhoph*, 1986).

Since the early '80s, physical methods have been developed (*Gautier et al.*, 1980; *Möser* and *Raschke*, 1984). These methods use radiances measured by instruments onboard satellites and related fluxes considering optical cloud properties, obtained by radiative transfer calculations. At present, surface flux components can be described by more complex methods, like the one by *Laszlo* and *Pinker* (1993).

Concerning the longwave (LW) component of the radiation budget, no simple relations like in the shortwave part are possible. Nevertheless, these methods are sensitive to the individual cloud types, their height and optical thickness, and temperature and humidity profiles in the atmosphere. All these methods are based on physical assumptions and have been applied to different data sets, like TOVS (*Gupta*, 1989), METEOSAT data combined with

meteorological measurements (*Schmetz*, 1984), or METEOSAT and ERBE data (*Stuhlmann*, 1993).

Three satellite-based radiation budget dataset are available on world wide web (*Bess et al.*, 2000). The dataset for ERBE is a 5-year monthly average time series from February 1985 through December 1989. The SRB dataset from July 1983 through June 1991 includes surface downward shortwave fluxes, surface downward longwave fluxes, surface albedos, and cloud coverage.

A relatively simple method to determine radiation budget components at the surface was developed at the Satellite Research Laboratory of the Hungarian Meteorological Service. Visible digital images of METEOSAT 4 or 5 satellite received in the morning hours (8 or 9 UTC), around noon (11 or 12 UTC), and in the afternoon (14 or 15 UTC) at the Hungarian Meteorological Service were used to characterize the daytime cloudiness, and the night-time cloudiness was taken from infrared images received at 21, 24, and 03 UTC. The region of Hungary has been covered by a grid (53 × 35 grid points), and pixels of 10 × 10 km^2 areas have been averaged for computation of the radiation balance components.

Methodology of radiation computations has already been described elsewhere (*Rimóczi-Paál et al.*, 1997a,b, 1999), here we give just a brief introduction and also a remark on the only step which differs from the steps previously applied in the process.

The radiation balance at the surface was calculated as

$$RB = G\,(1 - RS) + (LD - LU), \tag{1}$$

where *RB* is the radiation balance of the surface; *G* is the global radiation, *RS* is the surface albedo; *LD* is the longwave radiation reaching the surface; *LU* is the longwave radiation emitted by the surface.

The global radiation was calculated by a revised empirical equation from the relative brightness:

$$G = G_0 - 3.4 - 8.15\,B, \tag{2}$$

where *G* (%) is the global radiation given in percents of the solar radiation at the top of the atmosphere, G_0 is the clear sky global radiation. The definition of the relative brightness, *B*, is published in *Rimóczi-Paál* (1985). The clear-sky global radiation and longwave radiation reaching the surface were calculated by the radiative transfer model adapted from Main Geophysical Observatory of St. Petersburg (*Karol* and *Frolkis*, 1984; *Práger* and *Kovács*, 1988). Temperature and humidity profiles are taken from radiosonde observations

of 8 nearby radiosonde stations, by inverse quadratic distance interpolation for the 53 × 35 grid points. The emission of the surface could be estimated using the Stefan-Boltzmann law. Monthly surface albedo was taken from *Dávid et al.* (1990).

Effect of the clouds on the longwave radiation was approximated by a modified multi-layer parameterization. Vertical air humidity profiles are investigated to identify break-points. If there is one single break-point, then longwave estimations consider one cloud-layer at that level. We have assumed that the cloudiness of this layer produces the relative brightness of the corresponding pixel. If there is more than one breakpoint of the humidity profile, cloudiness is evenly distributed between the 2 or 3 most significant break-points.

First, the observations from each month of the 1992–1996 period are averaged for each selected hours, and these more regularly varying values are, then, numerically integrated over the whole month. In this manner, mean daily components of the radiation balance are determined for each month. Multiplicating these values by the number of days in a month, we have the monthly sum of the calculated radiation balance components.

Our purpose is to derive climatically representative radiation maps, obtained from a larger number of years (e.g., 30). In satellite meteorology only a very few series can even approximate this period. Hence, stratified sampling considering the frequency of macrosynoptic types defined for the study area is applied (*Mika et al.*, 1994). Skill of stratification depends on the selected weather categories, therefore, instead of the original macrosynoptic types by *Péczely* (1957), which defined 13 classes from the sea-level pressure patterns in Central Europe, later a set of new weather types was derived from the macrotypes with respect to their cloudiness (C) and temperature (T) conditions (*Rimóczi-Paál et al.*, 1997b). In this modified version, each macrotype had been selected into one of the 3 × 3 weather types, defined according to their negative, average, or positive long-term mean conditional anomalies considered in areal average for Hungary.

The climatically representative mean M^* has been calculated by Eq. (3):

$$M^* = \sum_{i=1}^{K} M_i(x) p(i), \tag{3}$$

where M^* is the climatically representative mean, $M_i(x)$ is the conditional mean value in the sample, for macrotype i (not perfectly equal to m_i, not known in general), the a priori probabilities (i.e., climatically determined relative frequencies) of these macrotypes are p_i ($i=1,\ldots,K$).

4. Verification

For testing our computations, satellite derived radiation balance terms of the corresponding 10 × 10 km^2 area were compared to the observed 10-minute averages at the BSRN station Budapest-Lőrinc. This BSRN station has been measuring the components of the radiation balance continuously with the same instrument since 1994. Thus, the verification has been carried out for the period 1994–1996. Results of this comparison are presented in *Tables 1* and *2*.

This investigation shows that correlations between traditional measurements and satellite-based estimations are generally fairly good. Characteristic values of the correlation coefficient are 0.6–0.9 as demonstrated in *Tables 1* and *2*. The correlation is generally higher in the cloudless situations, but this behavior is not clearly reflected in the annual cycles. Sample size is 94–1052 in case of global radiation and 510–1509 for the net radiation.

Mean systematic differences (biases) are almost always positive – that is the estimated values are higher than the measured ones – in all components of the radiation balance (including also those which are not displayed in *Tables 1* and *2*). Characteristic values of the bias are 10–20 J cm^{-2} for the global radiation demonstrated in *Table 1*. In case of high cloud coverage, defined by relative brightness values between 6 and 10, there is a strong under-estimation of the global radiation. In the case of net radiation, this bias is comparable to the observed averages.

Table 1. Results of the verification of the global radiation of point-wise surface observations at the Budapest-Lőrinc BSRN station and the corresponding METEOSAT-based 10 × 10 km^2 estimations (1994–1996). Seasonal subsamples and those according to the cloud amount (relative brightness) are presented. N – number of observations; Mean – observed average at the station (J cm^{-2}); SD – standard deviation (J cm^{-2}); Bias – average difference (J cm^{-2}); RMS – root mean square error (J cm^{-2}); Corr – correlation

	Global radiation					
	N	**Mean**	**SD**	**Bias**	**RMS**	**Corr**
			Cloud categories			
0–2	1052	183.3	87.7	14.9	45.5	0.87
2–4	312	117.2	81.0	17.5	60.2	0.70
4–6	179	98.1	70.5	2.1	57.1	0.58
6–10	94	82.9	67.5	-28.9	61.6	0.60
			Seasons			
Winter	237	80.5	49.3	7.1	28.9	0.85
Spring	541	158.4	88.2	11.4	50.3	0.83
Summer	660	199.8	86.4	10.8	22.7	0.75
Autumn	199	91.2	56.4	19.3	44.0	0.72
			Whole sample			
All	1637	155.6	91.8	11.5	51.0	0.84

Table 2. Results of the verification of the net radiation of point-wise surface observations at the Budapest-Lőrinc BSRN station and the corresponding METEOSAT-based 10 × 10 km^2 estimations (1994–1996). Seasonal subsamples and those according to the cloud amount (relative brightness) are presented. N – number of observations; Mean – observed average at the station (J cm^{-2}); SD – standard deviation (J cm^{-2}); Bias – average difference (J cm^{-2}); RMS – root mean square error (J cm^{-2}); Corr – correlation

	Net radiation					
	N	**Mean**	**SD**	**Bias**	**RMS**	**Corr**
Cloud categories						
0–2	1569	58.8	71.3	25.6	40.9	0.93
2–4	685	19.5	52.0	18.4	33.9	0.86
4–6	510	9.6	43.6	11.2	27.3	0.82
6–10	679	-1.9	27.0	11.2	22.1	0.73
Seasons						
Winter	564	4.6	28.1	16.8	23.2	0.82
Spring	965	40.6	65.6	22.6	37.6	0.92
Summer	1220	50.4	74.1	20.1	40.5	0.91
Autumn	694	8.9	37.9	15.0	25.8	0.87
Whole sample						
All	3443	31.8	62.7	19.2	34.6	0.82

Characteristic values of the RMS error of global radiation are between 23 and 60 J cm^{-2}. Net radiation is estimated by 22–40 J cm^{-2} RMS errors exhibiting annual cycle parallel to the mean value. Root-mean square errors for the net radiation (*Table 2*) are also comparable with the observed averages, which means that our algorithm can not be considered as the final approximation. As concerns the 5-year averages, either arithmetic or stratified, the substantial number of sample elements supporting the hourly estimations, the random error can already be just a minor part of its (unknown) real value.

Monthly totals were calculated by numerical integration for the period 1994–1996 and they were compared to measurements of BSRN station of Budapest. Both surface and satellite data were available in 33 months in this period. Using results of the validation at the calculation of the monthly total radiation matrices, the hourly values were corrected by the mean bias error for the actual month before the numerical integration, thus, significant over-estimation could not occur.

The comparison of the satellite-derived and measured monthly totals of the radiation balance components is presented in *Table 3*. Very good agreement could not be expected because of the integration approximation from the 4–8 hourly matrices per day. Inspite of this fact, it seems from *Table 3* that the Bias and RMS errors became much more lower than in the case of the hourly values. It can be concluded, that our method is suitable for the calculation of the monthly sums of the radiation balance components.

Table 3. Verification of monthly sums of the radiation budget components of point-wise surface observations at the Budapest-Lőrinc BSRN station and the corresponding METEOSAT-based 10 × 10 km^2 estimations (1994–1996). Seasonal subsamples and those according to the cloud amount (relative brightness) are presented. N – number of observations; Mean – observed average at the station (MJ m^{-2} month^{-1}); SD – standard deviation (MJ m^{-2} month^{-1}); Bias – average difference (MJ m^{-2} month^{-1}); RMS – root mean square error (MJ m^{-2} month^{-1}); Corr – correlation

Monthly amounts of the radiation budget components						
Component	**N**	**Mean**	**SD**	**Bias**	**RMS**	**Corr**
Global radiation	33	363.2	205.6	6.9	69.3	0.97
SW balance	33	279.3	166.6	12.1	58.8	0.96
Down longwave	33	786.0	161.8	20.4	66.9	0.92
LW balance	33	-149.1	77.3	-35.7	78.5	0.62
Net radiation	33	118.3	124.9	40.8	57.3	0.95

5. Results of monthly mapping

The above computations were performed for all months and radiation balance components by applying both schemes of averaging. In both cases first means of each hour were calculated, then the monthly sums were derived by numerical integration. In the case of climatically representative means, the individual hourly values were weighted by the relative frequency of the actual macro-synoptic type. There is no place and also no motivation to show all the digital maps, so we limit ourselves to the two main components, the global and net radiation. In consistency with the previous figures, maps of the global radiation in July (*Fig. 6*) and net radiation in January (*Fig. 7*) are presented in this paper. In the new National Climatic Atlas of Hungary (2001) normal average sums of the global radiation and net radiation in central months of the four seasons are published. Let us remind the reader that the resolution of the estimations is 10 × 10 km^2.

Comparing the maps prepared by the two different ways of averaging, one can establish a general similarity between the patterns in both pairs of demonstrated maps. This can be explained either by the inefficiency of the applied macrosynoptic classification or by the sufficient duration of the five years for climatic mapping. Since the macrotypes are grouped with respect to the conditional averages of cloudiness and near-surface temperature, we consider the second interpretation to be more likely. There are numerical differences between the two maps in July and January, too. Of course this is just a casual feature of the circulation anomalies in the particular period as compared to the 1961–1990 climate normal period. Among the presented pair

of maps, the net radiation patterns differ the most, as their magnitudes have the smallest absolute value, accompanied by relatively high RMS deviations, considered by the two averaging processes differently.

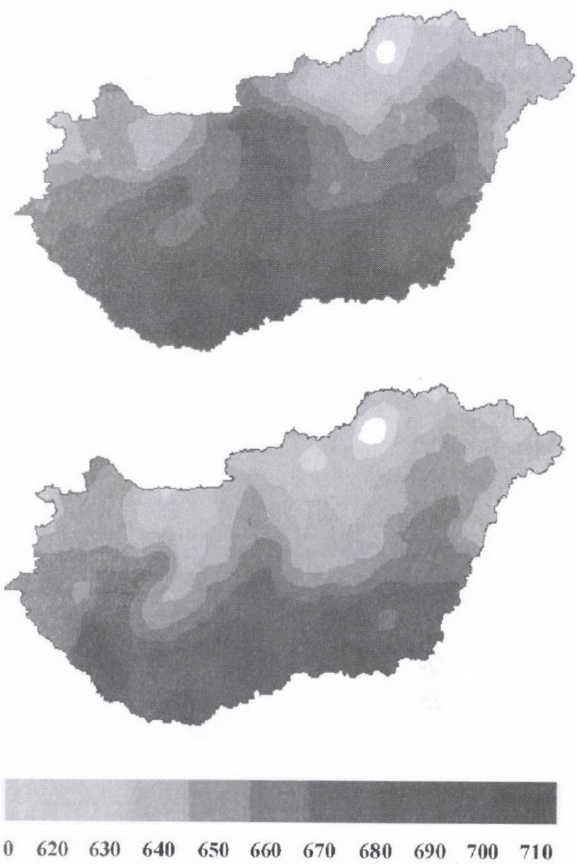

Fig. 6. Global radiation in July using METEOSAT data (MJ m^{-2}).
Top: 1992-1996. Bottom: climatically representative mean.

Comparing the new satellite-based radiation maps to the traditional maps one can establish that the "basin feature" in the global radiation does not appear as clearly in the new maps as one can be seen in the previous maps. The reason of this difference can be the circulation anomalies in the particular period. The new maps of the net radiation are much more detailed than the traditional maps.

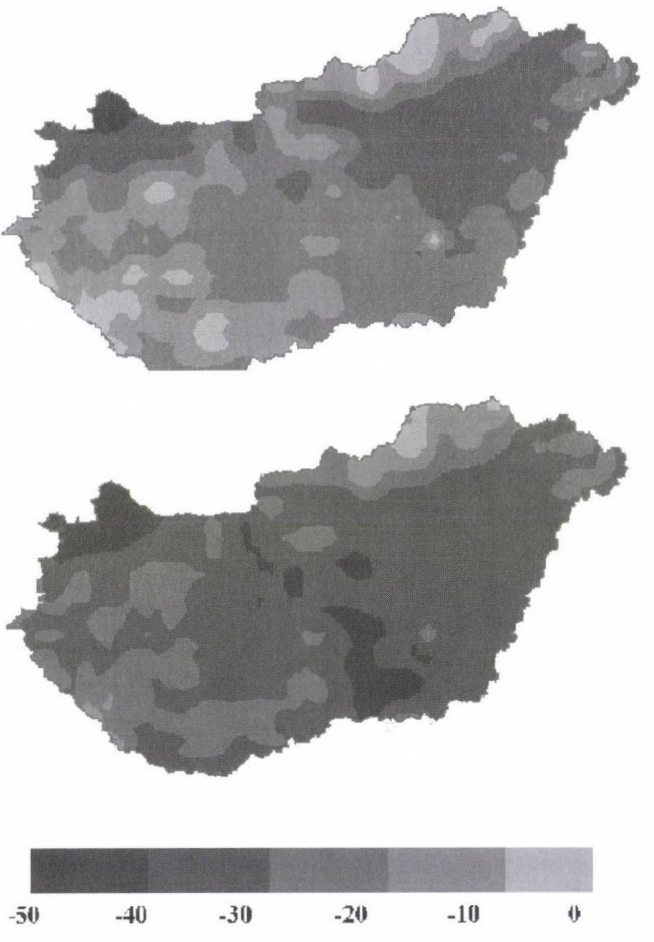

Fig. 7. Net radiation in January using METEOSAT data (MJ m^{-2}).
Top: 1992–1996. Bottom: climatically representative mean.

6. Summary

- Traditional radiation maps of Hungary are summarized.
- Our method to determine satellite-based radiation maps is shortly reviewed.
- Results of the validation are listed.
- Spatial distribution of the global radiation in July and that of the net radiation in January are presented by using two kinds of averaging.

- The new satellite-based radiation maps are much more detailed than the previous traditional radiation maps, and the "basin feature" can not be found as significantly as in the case of the previous maps.
- New operational method has been producing eight radiation matrices every day since the beginning of 2003.

Acknowledgements—The study was supported by the National Long-Term Research Fund (OTKA-T014933 and T025543) and Hungarian Space Agency (TP 088/2001-2002). Great thanks *Dr. János Mika* for the idea and determination of the climatically representative hourly radiation matrices, and *Dr. Roger Randriamampianina* for the Fortran program for the spatial interpolation of the humidity and temperature profiles.

References

Bess, T.D., Carlson, A.B., Mackey, C., Denn, F.M., Wilber, A., and *Rithley, N.*, 2000: World wide web access to radiation dataset for environmental and climate change studies. *B. Am. Meteorol. Soc. 81*, 2645-2652.

Brisson, A., Le Borgne, P., Marsoiun, A.,and *Moreaau, T.*, 1994: Surface irradiances calculated from Meteosat sensor data during SOFIA-STEX. *Int. J. Remote Sens. 15*, 197-205.

Dávid, A., Takács, O., and *Tiringer, Cs.*, 1990: *Distribution of the Radiation Balance in Hungary in the Period of 1951-1980* (in Hungarian). Országos Meteorológiai Szolgálat Kisebb Kiadványai, No. 66., Budapest.

Dobosi, Z. and *Takács, L.*, 1959: Spatial distribution of the global radiation in Hungary (in Hungarian). *Időjárás 63*, 82-84.

Eymard, L. and *Taconet, O.*, 1995: The methods inferring surface fluxes from satellite data, and their use for atmosphere model validation. *Int. J. Remote Sens. 16*, 1907-7930.

Fritz, S. and *Rao, K.P.*, 1967: On the infrared transmission through cirrus clouds and the estimation of relative humidity from satellites. *J. Appl. Meteorol. 6*, 1088-1096.

Gautier, C., Diak, G., and *Masse, S.*, 1980: Simple physical model to estimate incident solar radiation from GOES satellite data. *J. Clim. Appl. Meteorol. 19*, 1005-1012.

Gupta, S.K, 1989: A parameterization for longwave surface radiation from Sun-synchronous satellite data. *J. Climate 2*, 302-315.

Karol, I.L. and *Frolkis, A.A.*, 1984: Energy-balance type radiative-convective model of global climate (in Russian). *Meteorology and Hydrology*, No. 8, 59-68.

Klink, J.C. and *Dollhopf, K.J.*, 1986: An evaluation of satellite-based insolation estimates for Ohio. *J. Clim. Appl. Meteorol. 25*, 1741-1751.

Laszlo, I. and *Pinker, R.T.*, 1993: Shortwave cloud-radiative forcing at the top of the atmosphere, at the surface and of the atmospheric column as determined from ISCCP C1 data. *J. Geophys. Res. 98(D2)*, 2703-2713.

Major, Gy., (ed.), 1976: *The Solar Radiation in Hungary, 1958-1972* (in Hungarian). Orsz. Meteorológiai Szolgálat Hivatalos Kiadványa. Magyarország éghajlata, No. 10, Budapest.

Major, G. and *Takács, O.*, 1985: Main characteristics of solar irradiation in Hungary. *Int. Agrophysics 1*, 67-73.

Mika, J., Szentimrey, T., Domonkos, P., Rimóczi-Paál, A., and *Károssy, C.*, 1994: Approximating climatic representativity for satellite samples of limited length. *Adv. Space Res. 14*, 125-128.

Möser, W. and *Raschke, E.*, 1984: Incident solar radiation over Europe from METEOSAT data. *J. Clim. Appl. Meteorol. 23*, 166-170.

Péczely, G., 1957: *Grosswetterlagen in Ungarn.* Kleinere Veröffentlichungen der Zentralanstalt für Meteorologie. Nr. 30, Budapest.

Práger, T. and *Kovács, E.*, 1988: Estimation of climate forcing effects of atmospheric gases and aerosols by radiative-convective model (in Hungarian). *Időjárás 92*, 153-162.

Rimóczi-Paál, A., 1985: Determination of surface global radiation using relative brightness as new parameter to characterize the cloudiness. *Adv. Space Res. 5*, No. 6., 329-333.

Rimóczi-Paál, A., Randriamampianina, R., and *Gyarmati, Gy.*, 1997a: Radiation balance investigations using METEOSAT data. In *International Radiation Symposium*. Fairbanks, Alaska, 19-24 August, 1996, 1049-1052.

Rimóczi-Paál, A., Mika, J., Szentimrey, T., Csiszár, I., Gyarmati, G., Domonkos, P., and *Károssy, C.*, 1997b: Estimation of surface radiation balance components from METEOSAT images: Five years statistics. *Adv. Space Res. 19*, 473-476.

Rimóczi-Paál, A., Kerényi, J., Mika, J., Randriamampianina, R., Dobi, I., Imecs, Z., and *Szentimrey, T.*, 1999: Mapping daily and monthly radiation components using METEOSAT data. *Adv. Space Res. 24*, 967-970.

Schmetz, J., 1984: On the parameterisation of the radiative properties of broken cloud. *Tellus 36A*, 417-432.

Schmetz, J., 1989: Towards a surface radiation climatology: Retrieval of downward irradiances from satellite. *Atmos. Res. 23*, 287-321.

Sellers, P.J., Rasool, S.I., and *Bolle, H.-J.*, 1990: A Review of Satellite Data Algorithms for Studies of the Land Surface. *B. Am. Meteorol. Soc. 71*, 1429-1447.

Stuhlmann, R., 1993: Feasibility study for calculating the cloud-generated radiative flux divergence from METEOSAT imagery data. *Technical Report*. Institut für Physik II/PC, GKSS-Forschungszentrum. Geesthacht, Germany.

Takács, O., 1974: Spatial distribution of the global radiation using measured data in Hungary (in Hungarian). *Beszámolók az 1971-ben végzett tudományos kutatásokról*. Országos Meteorológiai Szolgálat, Budapest, 251-256.

Tarpley, J., 1979: Estimating incident solar radiation at the surface from geostationary satellite data. *J. Appl. Meteorol. 18*, 1172-1181.

GUIDE FOR AUTHORS OF *IDŐJÁRÁS*

The purpose of the journal is to publish papers in any field of meteorology and atmosphere related scientific areas. These may be

- research papers on new results of scientific investigations,
- critical review articles summarizing the current state of art of a certain topic,
- short contributions dealing with a particular question.

Some issues contain "News" and "Book review", therefore, such contributions are also welcome. The papers must be in American English and should be checked by a native speaker if necessary.

Authors are requested to send their manuscripts to

Editor-in Chief of IDŐJÁRÁS
P.O. Box 39, H-1675 Budapest, Hungary

in three identical printed copies including all illustrations. Papers will then be reviewed normally by two independent referees, who remain unidentified for the author(s). The Editor-in-Chief will inform the author(s) whether or not the paper is acceptable for publication, and what modifications, if any, are necessary.

Please, follow the order given below when typing manuscripts.

Title part: should consist of the title, the name(s) of the author(s), their affiliation(s) including full postal and E-mail address(es). In case of more than one author, the corresponding author must be identified.

Abstract: should contain the purpose, the applied data and methods as well as the basic conclusion(s) of the paper.

Key-words: must be included (from 5 to 10) to help to classify the topic.

Text: has to be typed in double spacing with wide margins on one side of an A4 size white paper. Use of S.I. units are expected, and the use of negative exponent is preferred to fractional sign. Mathematical formulae are expected to be as simple as possible and numbered in parentheses at the right margin.

All publications cited in the text should be presented in a *list of references*, arranged in alphabetical order. For an article: name(s) of author(s) in Italics, year, title of article, name of journal, volume, number (the latter two in Italics) and pages. E.g., *Nathan, K.K.,* 1986: A note on the relationship between photo-synthetically active radiation and cloud amount. *Időjárás 90,* 10-13. For a book: name(s) of author(s), year, title of the book (all in Italics except the year), publisher and place of publication. E.g., *Junge, C. E.,* 1963: *Air Chemistry and Radioactivity.* Academic Press, New York and London. Reference in the text should contain the name(s) of the author(s) in Italics and year of publication. E.g., in the case of one author: *Miller* (1989); in the case of two authors: *Gamov* and *Cleveland* (1973); and if there are more than two authors: *Smith et al.* (1990). If the name of the author cannot be fitted into the text: *(Miller,* 1989); etc. When referring papers published in the same year by the same author, letters a, b, c, etc. should follow the year of publication.

Tables should be marked by Arabic numbers and printed in separate sheets with their numbers and legends given below them. Avoid too lengthy or complicated tables, or tables duplicating results given in other form in the manuscript (e.g., graphs)

Figures should also be marked with Arabic numbers and printed in black and white in camera-ready form in separate sheets with their numbers and captions given below them. Good quality laser printings are preferred.

The text should be submitted both in manuscript and in electronic form, the latter on diskette or in E-mail. Use standard 3.5" MS-DOS formatted diskette or CD for this purpose. MS Word format is preferred.

Reprints: authors receive 30 reprints free of charge. Additional reprints may be ordered at the authors' expense when sending back the proofs to the Editorial Office.

More information for authors is available: antal.e@met.hu

Information on the last issues: http://omsz.met.hu/irodalom/firat_ido/ido_hu.html

Published by the Hungarian Meteorological Service

Budapest, Hungary

INDEX: 26 361

HU ISSN 0324-6329